

# Parallel signaling pathways regulate excitable dynamics differently for pseudopod formation in eukaryotic chemotaxis

**Authors:** Yuki Tanabe<sup>1,2</sup>, Yoichiro Kamimura<sup>2</sup> & Masahiro Ueda<sup>1,2,3\*</sup>

## **Affiliations:**

<sup>1</sup>Laboratory of Single Molecular Biology, Department of Biological Sciences, Graduate School of Science, Osaka University, Toyonaka, Osaka, 560-0043, Japan

<sup>2</sup>Laboratory for Cell Signaling Dynamics, Center for Biosystems Dynamics Research (BDR), RIKEN, Suita, Osaka, 565-0874, Japan

<sup>3</sup>Laboratory of Single Molecule Biology, Graduate School of Frontier Biosciences, Osaka University, Suita, Osaka 565-0871, Japan

Key words: cGMP signaling, chemotaxis, excitability, pseudopod formation

\*Corresponding author

Masahiro Ueda,

Graduate School of Frontier Biosciences, Osaka University

Suita, Osaka 565-0871, Japan.

E-mail: masahiroueda@fbs.osaka-u.ac.jp

## Abstract

In eukaryotic chemotaxis, parallel signaling pathways regulate the spatiotemporal pseudopod dynamics at the leading edge of a motile cell through characteristic dynamics of an excitable system; however, differences in the excitability and the physiological roles of individual pathways remain to be elucidated. Here we found that two different pathways, soluble guanylyl cyclase (sGC) and phosphatidylinositol 3-kinase (PI3K), exhibited similar all-or-none responses but different refractory periods by simultaneous observations of their excitable properties. Due to the shorter refractory period, sGC signaling responded more frequently to chemoattractants, leading to pseudopod formation with higher frequency. sGC excitability was regulated negatively by its product, cGMP, and cGMP-binding protein C (GbpC) through the suppression of F-actin polymerization, providing the underlying delayed negative feedback mechanism for the cyclical pseudopod formation. These results suggest that parallel pathways respond on different time-scales to environmental cues for chemotactic motility based on their intrinsic excitability.

## Introduction

Chemotaxis to extracellular chemical signals plays important roles in various physiological phenomena including neurogenesis, immune response and wound healing (Servant et al., 2000; Kalil and Dent, 2005; Mayor and Etienne-Manneville, 2016). Chemotactic cells, such as mammalian neutrophils and social amoeba *Dictyostelium discoideum*, detect chemical gradients and migrate directionally by coordinating their anterior pseudopod formation and posterior tail contraction (Van Haastert and Devreotes, 2004; Hind et al., 2016).

Evolutionally conserved molecular mechanisms are involved in the bias of cell motility directionally along chemoattractant gradients (Artemenko et al., 2017; Devreotes et al., 2017). In *Dictyostelium* cells, extracellular 3',5'-cyclic adenosine monophosphate (cAMP) works as a chemoattractant and is detected by G protein coupled receptor (GPCR) and cognate heterotrimeric G-proteins. This detection activates multiple signaling pathways including those of PI3K-PTEN, PLA2, TorC2-PDK-PKB, and soluble guanylyl cyclase (sGC). Most of these parallel and compensatory pathways generate a polarized signal selectively at the front or back of a motile cell along the cAMP gradient (Cai and Devreotes, 2011; Artemenko et al., 2014; Devreotes et al., 2017). In the PI3K-PTEN pathway, a phosphatidylinositol 3,4,5-trisphosphate (PIP3)-enriched domain localizes to the pseudopod and regulates the polymerization or stabilization of F-actin (Kortholt et al., 2011; Devreotes et al., 2017). Similar localizations of sGC and PKB activities also act as intracellular cues for pseudopod formation (Veltman and Van Haastert, 2006; Kamimura et al., 2008). However, little is known about the relations between the parallel signaling pathways and their unique functions for chemotaxis.

The spatiotemporal dynamics of PIP3 has been well characterized for the chemotactic motility of eukaryotic amoeboid cells such as *Dictyostelium*. A PIP3-enriched domain on the membrane is produced in a self-organized manner independent of cell motility and shows wave-like localization patterns (Asano et al., 2008; Arai et al., 2010; Gerisch et al., 2012). The PIP3-enriched domain spontaneously occurs in the absence of extracellular stimuli, and it has relatively constant biochemical activities and size of a few microns in diameter. These spontaneous activities are linked to pseudopod formation and are biased along cAMP gradients, leading to a change from random to directional motility (Xiong et al., 2010; Shibata et al., 2013). The PIP3 dynamics has been explained by an intrinsic excitable system. In general, an excitable system shows an all-or-none response to a super-threshold stimulus so that constant output independent of the input strength is assured (Huang et al., 2013; Nishikawa et al., 2014). Thus, the excitable behavior is able to amplify the small input and function as an internal biochemical compass of motile cells (Xiong et al., 2010; Shibata et al., 2013). Human neutrophils also exhibit excitability for PIP3 on the membrane, suggesting a conserved property for eukaryotic chemotaxis (Tang et al., 2014). Another feature of excitability is characterized by the refractory period, which is the recovery time for the system

to react to a second stimulus once its excitation starts. During the refractory state, the system cannot respond even to a stimulus beyond the threshold. Thus, excitability determines the responsiveness of a cell to the environmental stimulus. The PIP3 pathway in *Dictyostelium* cells has a refractory period of around 60 sec (Huang et al., 2013; Nishikawa et al., 2014), which is longer than the time scale at which cells respond to chemical gradients, giving ambiguity to the physiological meaning of the refractory period.

Among parallel pathways, the sGC pathway has been well documented to contribute to the chemotaxis of *Dictyostelium* cells (Veltman et al., 2008). A series of mutants in the sGC pathway have been shown to impair chemotaxis to various kinds of chemoattractants including cAMP and folic acids, demonstrating the importance of the pathway in chemotactic signaling (Kuwayama et al., 1993, 1995). In the sGC pathway, extracellular cAMP induces intracellular cGMP elevation, which serves as a second messenger for tail contraction at the posterior of the cell via the regulation of myosin II (MyoII) (Soll et al., 2009). cGMP is synthesized by two different types of guanylyl cyclase, cytosolic sGC and membrane-embedded guanylyl cyclase A (GCA) (Roelofs et al., 2001, 2002). sGC mainly contributes to guanylyl cyclase activity during the cell aggregation stage at around 5 hours after starvation. Bioinformatic analysis has discovered four cGMP-binding candidate proteins, GbpA-D (Goldberg et al., 2002). All four proteins have cyclic nucleotide binding motifs, but biochemical experiments revealed that GbpC is a major cGMP effector (Bosgraaf et al., 2002). The degradation of cGMP is catalyzed by two cGMP phosphodiesterases, GbpA and GbpB (Bosgraaf et al., 2002). On the other hand, GbpC serves as the intracellular high-affinity binding site for cGMP and is required for MyoII regulation, while GbpD regulates cell adhesion through its guanine nucleotide exchange factor (GEF) activity for Rap1 even though it has no cGMP binding ability (Bosgraaf et al., 2005; Kortholt et al., 2006). In addition to the regulation of MyoII at the posterior tail, it has been suggested that the sGC pathway has additional function at the pseudopod (Veltman et al., 2005). sGC proteins localize to pseudopods through the N terminus without the enzymatic domain during random and chemotactic migration, and cAMP stimulations induce transient recruitments of sGC to the membrane in a manner similar to PIP3 dynamics (Veltman and Van Haastert, 2006). Cells lacking the N terminus of sGC exhibit a high degree of turning, which brings about a loss of cell orientation, an effect similarly seen in *pi3k1, 2* double knockout strains (Bosgraaf and Van Haastert, 2009). These observations suggest that the sGC pathway has characteristics of an excitable system, however, no direct evidence has been obtained experimentally.

Here we found that sGC and PIP3 show pseudopod localizations at different frequencies in individual cells and demonstrated that sGC localization shows behavior consistent with an excitable system including an all-or-none response to cAMP stimulation, wave-like pattern formation and refractory period. The refractory period of the sGC-mediated signaling pathway was shorter than that of PIP3, and sGC localized to the pseudopod more frequently than PIP3. sGC localization depended on F-actin and was negatively regulated by cGMP and GbpC via F-actin dynamics, indicating that sGC localization and F-actin are incorporated into one excitable network. This regulation explains the short sGC refractory period as well as concomitant pseudopod formation with relatively high frequency. Overall, these results illustrate that multiple signaling pathways regulate pseudopod dynamics differently through their characteristic excitable properties for chemotactic motility.

## Results

### Multiple signaling pathways have unique dynamics in localization patterns for cell migration.

To address how parallel pathways regulate cell migration, we observed the localization patterns of sGC and PIP3 simultaneously in individual cells. Since sGC localizes to pseudopods through its N-terminal region, we used its Halo-tagged protein as a sGC probe (sGC<sub>N</sub>-Halo) along with a previously reported PIP3 probe, the GFP tagged pleckstrin homology domain of *Dictyostelium* PKBA (PH<sub>PKB</sub>-GFP) (Meili et al., 1999; Veltman and Van Haastert, 2006; Asano et al., 2008). sGC<sub>N</sub>-Halo was stained by tetramethylrhodamine (TMR) for multicolour imaging. In wild-type cells co-expressing sGC<sub>N</sub>-Halo and PH<sub>PKB</sub>-GFP, sGC<sub>N</sub> signals were observed in all pseudopods, while PIP3 signals were observed in only half (Fig. 1A, S1A). Statistical analysis revealed that the localization pattern was classified into three types: pseudopods with sGC<sub>N</sub> localization alone (47.8%), with sGC<sub>N</sub> and PIP3 co-localization (50.2%) and with PIP3 alone (2.0%) (n = 452 pseudopods from 13 cells) (Fig. 1B). We analyzed several parameters of the pseudopod dynamics, including extended length, life-time, contribution to cell movement, and appearance frequency, for each localization pattern by measuring the extended area of the spontaneously formed pseudopods (see Materials and Methods, Fig. S1B). While small extensions were observed in pseudopods with sGC alone, pseudopods with sGC and PIP3 co-localization were coupled with larger extensions (Fig. 1C, D). In fact, the elongation length of pseudopods with sGC and PIP3 co-localization ( $5.22 \pm 2.31 \mu\text{m}$ , n= 189 pseudopods) was higher than that of sGC alone ( $3.92 \pm 1.79 \mu\text{m}$ , n= 147 pseudopods) (Fig. 1E). To see the sole effect of sGC localization on the pseudopod dynamics, we created *sgcΔ* cells, which express a mutant sGC lacking its N-terminal region (sGC $\Delta$ N-Halo/*sgcΔ*) but maintains the catalytic domain for cGMP synthesis. PIP3-alone

pseudopods in these mutant cells exhibited small elongations compared to those of sGC and PIP3 co-localized pseudopods ( $4.28 \pm 2.16 \mu\text{m}$ ,  $n=61$  pseudopods, vs.  $5.22 \pm 2.31 \mu\text{m}$ ,  $n=189$ ). Wild-type cells treated with LY294002, a pharmacological PI3K inhibitor, exhibited only small elongations ( $2.82 \pm 1.08 \mu\text{m}$ ,  $n=39$  pseudopods) (Fig. 1E). Consistently, the life-time and the contribution to cell motility of pseudopods with both signals were higher than those with sGC alone (Fig. S1C, D). However, the appearance frequency was not significantly different (Fig. S1E). These genetic and pharmacological inhibitions also caused decreases in the velocity of random migration (Fig. S1F). These observations suggest that the two parallel pathways regulate pseudopod formation additively.

We next observed both signaling molecules under cAMP gradients to see how their pathways regulate pseudopod formation in chemotaxis (Fig. 1F, G and Movie 1). Upon uniform cAMP stimulation, both signaling molecules exhibited a transient localization to the membrane independently of one other (Fig. S1G, H), demonstrating that the two pathways work in parallel. Under cAMP gradients, the localization patterns of both signaling molecules exhibited different characteristic dynamics (Fig. 1F, G and Movie 1). When the source of the chemoattractant gradient was continuously moved around the cell, sGC and PIP3 were able to follow the changes of the position similarly (Fig. 1F, S1I). On the other hand, once the source position was fixed, the membrane localization of sGC and PIP3 behaved differently (Fig. 1G). The stimulus at first induced sGC and PIP3 localization to the same pseudopod and was followed by a transient disappearance of both signals. Later sGC localization preceded PIP3 localization on the pseudopod, showing that sGC localized to the pseudopod more frequently than PIP3, consistent with the observations in randomly moving cells (Fig. 1A, B). These results demonstrate that both signaling pathways have their own unique dynamics to the same cAMP stimulation.

### **sGC localization follows the all-or-none law**

We next determined whether sGC localization has the features of excitability or not. An excitable system shows the same response to any perturbation over a certain threshold because the response is determined by an intrinsic excitable mechanism. We expected that a pulse cAMP stimulus with a very short-duration could trigger the same response in sGC localization as a stepwise cAMP stimulus if the responses are excitable. For this purpose, we used an experimental system in which caged-cAMP was photolyzed in a flow chamber, allowing us to control the timing and strength of the pulse stimuli by manipulating the exposure times of UV irradiation (Fig. S2A) (Beta et al., 2007). Upon UV flash at a region upstream of the cells, the uncaged cAMP was applied to and removed from the cells within a few seconds by the flow (Fig. S2B), which is short enough to test the excitability of sGC localization (Veltman et al., 2005). The C-terminal fusion of GFP to full-length sGC (sGC-GFP) was expressed in *gcl*

cells lacking both sGC and GCA, and sGC-GFP localization was observed in response to the transient stimulation. Cytosolic sGC-GFP exhibited translocation to the membrane as a transient response to a pulse stimulus within 2 sec of UV exposure as well as a step stimulus of 100 nM cAMP (Fig. 2A). The two transient responses had the same temporal changes and same peak amplitude, indicating that the sGC localization dynamics is produced intrinsically by the system itself in a manner independent of the stimulus pattern. Furthermore, we examined the dose-dependent response of sGC localization to the membrane by various exposure times of UV light. As expected, the cells expanded the domain size of the sGC signals on the membrane with increasing levels of activated cAMP, although the domain amplitudes remained constant (Fig. 2B). To confirm that the uncaging by UV-flash provided the expected cAMP concentrations precisely, we uniformly stimulated the cells with the defined cAMP concentrations and observed sGC-GFP translocation to the membrane. Similar to Fig. 2B, the domain size on the membrane increased according to the cAMP concentration until 0.1 nM with constant domain amplitudes (Fig. S2C). These results reflect excitable features such as stimulus-dependent domain size and constant amplitude, which were observed in PIP3 excitation previously (Nishikawa et al., 2014).

An excitable system often shows wave-like propagation (Sager, 1996; Khamviwath et al., 2013). In *Dictyostelium* cells, PIP3 and F-actin accumulations on the membrane are typical examples of travelling wave generation (Arai et al., 2010; Gerisch et al., 2011). When we mildly perturbed the actin cytoskeleton with a low concentration of latrunculin A, an actin polymerization inhibitor, we found F-actin showed wave-like propagation on the bottom surface of the cells, as visualized by the fluorescent F-actin probe mRFP-LimE $\Delta$ coil (Fig. 2C) (Fischer et al., 2004). The same behavior was observed for sGC-GFP localization, which overlapped the F-actin signals (Fig. 2C, Movie 2). Furthermore, cAMP-elicited sGC localization to the membrane was significantly reduced in mutant cells lacking functional ArcB, a subunit of Arp2/3 complex, which is responsible for actin polymerization (Fig. 2D) (Langridge and Kay, 2007). Overall, these results imply that the excitable behavior of sGC relies on F-actin activity.

### **sGC shows a unique refractory period that is shorter than that of PIP3**

We determined whether sGC localization to the membrane exhibits a refractory period or not. *gcA* cells expressing full length sGC-GFP were stimulated repeatedly with pulsed cAMP at different time intervals (Fig. 3A, B). Transient recruitment of sGC-GFP in response to repetitive stimuli at 21-sec and 30-sec intervals occurred normally. However, in response to repetitive stimuli at 12-sec intervals, the first response was normal but the second and third responses were progressively weaker. These results indicate that the sGC localization has a



refractory period between 10-20 sec. The existence of the all-or-none response, propagating wave and refractory period proves the excitability of the sGC signaling pathway.

Next we compared the excitable properties of sGC and PIP3 localizations on the membrane. First, we directly evaluated their refractory times by observing cells that co-expressed both sGC<sub>N</sub>-Halo and PH<sub>PKB</sub>-GFP when stimulated repeatedly by UV-irradiation at 21-sec intervals. sGC localization exhibited a response repeatedly to all stimuli, whereas PIP3 did not (Fig. 3C). The refractory period of PIP3 localization was about 30-60 sec (Fig. 3D), consistent with previous reports (Huang et al., 2013; Nishikawa et al., 2014). sGC localized to the membrane in mutant cells lacking *pi3k1* and *pi3k2* genes upon repeated stimuli with a refractory period of 30 sec, indicating that sGC responsiveness to cAMP stimulation is independent of PIP3 production (Fig. 3E). Thus, the excitable dynamics of sGC has a unique refractory period that is shorter than that of PIP3. Therefore, the sGC pathway can respond to stimulations of short intervals (about 10-20 sec), but the PI3K-PTEN pathway cannot.

### **cGMP-binding protein, GbpC, suppresses sGC accumulation on the membrane**

To gain molecular insights into the excitable behavior of the sGC pathway, we focused on the possible involvement of both the pathway's product, cGMP, and downstream signaling molecules, because excitable systems generally include a delayed negative feedback mechanism to generate transient excitation (Cao et al., 2016). To reveal the effect of cGMP on sGC localization to the membrane, we first observed mutant sGC with the amino acid change Asp1106Ala, which lacks catalytic activity (sGC $\Delta$ cat) and was previously expressed as a tagged protein with GFP (sGC $\Delta$ cat-GFP) in *gcA* cells (Veltman and Van Haastert, 2006; Sato et al., 2009). It was reported that *gcA* cells expressing sGC $\Delta$ cat upon cAMP stimulation fail to produce cGMP (Veltman and Van Haastert, 2006). Wild-type sGC-GFP (sGCwt-GFP) exhibited translocation to the membrane transiently upon cAMP stimulation, but the translocation terminated within 20 sec. On the other hand, the catalytically dead mutant sGC $\Delta$ cat-GFP showed prolonged and stronger membrane localization for several minutes (Fig. 4A), indicating that intracellular cGMP accelerates the dissociation of sGC from the membrane. As a control, we examined the response of sGC $\Delta$ cat-GFP in wild-type cells (Fig. S3A). sGC $\Delta$ cat-GFP showed translocation to the membrane upon cAMP stimulation in a similar manner to sGCwt-GFP. However, there were some differences in the behavior between sGCwt-GFP and sGC $\Delta$ cat-GFP after 30 sec of stimulation; much more sGCwt-GFP returned to the cytosol than sGC $\Delta$ cat-GFP, probably because the overproduction of sGCwt-GFP increases the cGMP level in wild-type cells. We also examined the cAMP-mediated responses of wild-type and *gcA* cells in which the C-terminal catalytic domain was deleted (sGC<sub>N</sub>-GFP; Fig. S3B). As expected from the data of Fig. 4A,



sGC<sub>N</sub>-GFP translocated to the membrane within 10 sec in both cells, but the returning phase to the cytosol was slower in *gcA* cells. Also, much more sGC<sub>wt</sub>-GFP dissociated from the membrane in wild-type cells than sGC<sub>N</sub>-GFP (compare Fig. S3A and S3B). When co-expressed in the same wild-type cells, sGC<sub>wt</sub> and sGC<sub>N</sub> revealed almost the same dynamics upon cAMP stimulation, reaching equivalent cytosolic levels (Fig. S3C). These results further implicate intracellular cGMP in the dissociation of membrane sGC.

Next, we observed wild-type sGC localization in a series of mutant cells lacking GbpA and GbpB (*gbpABΔ*), GbpC (*gbpCΔ*), or GbpD (*gbpDΔ*). Among them, only *gbpCΔ* cells exhibited defects in sGC-GFP localization, in which sGC-GFP continued to localize on the membrane stably in a manner similar to sGC $\Delta$ cat-GFP (Fig. 4B). The other mutants exhibited no obvious changes in sGC-GFP localization at resting state without cAMP stimulation (Fig. 4B). When stimulated with cAMP, *gbpCΔ* cells exhibited prolonged responses in sGC-GFP translocation to the membrane, while wild-type cells exhibited transient responses (Fig. 4C). Thus, sGC localization to the membrane is regulated negatively by its product, cGMP, and a cGMP-dependent signaling molecule, GbpC, which ensures the transient response of sGC localization upon cAMP stimulation. In addition, *mhcAΔ* cells, which lack myosin heavy chain, a gene required for cell contraction at the posterior side, exhibited transient responses of sGC localization on the membrane upon cAMP stimulation, although the activity was less efficient than in wild-type cells (Fig. 4C). These results demonstrate that cGMP-dependent GbpC signaling regulates negatively the lifetime of sGC accumulation on the membrane. Because sGC catalyzes cGMP production, this negative regulation by GbpC provides a delayed negative feedback loop for the sGC excitation pathway.

### **GbpC regulates the refractory period of the sGC pathway for fast pseudopod cycling**

The above results suggest that cGMP-dependent GbpC signaling suppresses sGC localization to the membrane and that this negative feedback regulates recovery to the basal state, that is the refractory period, in sGC excitation. In fact, sGC-GFP in *gbpCΔ* cells showed persistent but not repetitive responses to 12-sec and 21-sec interval stimuli (Fig. 5A), which resembles the response to step stimuli (Fig. 4C), indicating that cells require GbpC to distinguish repeated pulsatile stimuli from continuous stimuli. Because sGC-GFP in *gbpCΔ* cells responded to repetitive pulse stimuli at 30-sec intervals in a manner similar to sGC-GFP in wild-type cells (Figs. 3A and 5A), we can conclude that sGC excitation can recover to basal state within 30 sec in a GbpC-independent manner. Next, we observed sGC-GFP responses in a *gbpAΔ* cell line, in which the cGMP-specific phosphodiesterase gene is deleted, to see the effects of cGMP on the refractory period, because *gbpAΔ* cells are reported to show prolonged over-production of cGMP upon cAMP stimulation (Lusche and Malchow, 2005). The *gbpAΔ* cells showed severely suppressed sGC-GFP responses to repeated stimuli at

21-sec intervals, while wild-type cells responded normally (Figs. 3A and 5B). That is, prolonged cGMP overproduction prolonged the refractory period. Thus, cGMP-dependent GbpC signaling is required for shortening the refractory period and provides a mechanism for the fast recovery of the sGC pathway in order to respond to the subsequent cAMP stimulation.

To examine the effects of cGMP-dependent GbpC signaling on F-actin polymerization and pseudopod formation in response to cAMP stimulation, we observed mRFP-LimE $\Delta$ coil in *gcA* and *gbpA* $\Delta$  cells, which have defects in the production and degradation of cGMP, respectively (Figs. 5C, S4A and Movie 3). Wild-type cells showed transient F-actin polymerization at the entire cell surface at around 10 sec after continuous cAMP stimulation, which was followed by the formation of multiple pseudopods with F-actin polymerization for around 1 min, as observed by mRFP-LimE $\Delta$ coil localization. When *gbpA* $\Delta$  cells were exposed to the same stimulus, subsequent responses were not observed over the several-minute observation period, showing a long suppression of F-actin polymerization. The ectopic expression of GbpA in *gbpA* $\Delta$  cells rescued the delay of the secondary response (Fig. 5C, GbpA/*gbpA* $\Delta$ ).

To further confirm these results, we observed the refractory period in a repetitive stimuli experiment. *gbpA* $\Delta$  cells significantly reduced the second response to a 21-sec interval stimulus, while wild-type and rescued *gbpA* $\Delta$  cells revealed almost the same response to the first and second stimuli (Fig. S4B). On the other hand, both *gcA* and *gbpC* $\Delta$  cells exhibited enhanced F-actin polymerization (Fig. 5C, Movie 4). This persistent F-actin formation in *gbpC* $\Delta$  cells was also observed in a biochemical assay (Fig. 5D, S4C). GbpC has Ras-like Roc, RasGEF, and MAPKKkinase domains plus a cGMP-binding domain. It has been reported that cGMP binding to GbpC triggers intramolecular signal transduction, ultimately leading to kinase activation (Van Egmond et al., 2008). Therefore, we analyzed the involvement of this intramolecular signaling in GbpC-mediated F-actin regulation using deletion mutants of the MAPKKkinase or cGMP-binding domain. We found neither mutant was able to rescue the phenotype of excessive F-actin formation upon cAMP stimulation, suggesting that GbpC requires kinase activation following cGMP binding for this regulation (Fig. 5D). These results are consistent with cGMP-dependent GbpC signaling suppressing F-actin polymerization and pseudopod formation. Thus, the negative feedback from cGMP/GbpC to sGC shortens the refractory period of sGC localization to the membrane, which provides a mechanism for the high frequency, repetitive pseudopod formation upon cAMP stimulation.

## Discussion

Eukaryotic chemotaxis is mediated by parallel signaling pathways that have characteristic features of excitability for the generation of all-or-none signals to regulate pseudopod dynamics at the front of the cells (Cai and Devreotes, 2011; Devreotes et al., 2017). Previous reports have demonstrated PIP3 excitation on the membrane during the chemotactic signaling of *Dictyostelium* cells and neutrophil cells (Huang et al., 2013; Nishikawa et al., 2014; Tang et al., 2014). Here we demonstrated sGC localization to the membrane was consistent with excitable behaviors such as an all-or-none response (Fig. 2A, B, S2C), wave-like pattern formation (Fig. 2C) and refractory period (Fig. 3). These observations indicate the universality of excitable systems for chemotactic signaling pathways. Although both the PI3K-PTEN and sGC pathways have excitable properties, each pathway independently forms an excitable network, as shown by the following findings. First, sGC localization strongly relied on F-actin (Fig. 2D), but F-actin was not essential for PIP3 excitation on the membrane (Arai et al., 2010). Second, sGC responses upon pulse stimuli showed shorter refractory periods (10 ~ 20 sec) than PIP3 responses (30 ~ 60 sec) (Fig. 3C, D). Finally, the refractory period of sGC localization was independent of PIP3 production (Fig. 3E). These results indicate that each downstream pathway has unique characteristics for excitable dynamics.

Our observations revealed that sGC localized to the pseudopod more frequently than PIP3 when cells moved along the chemoattractant gradient (Fig. 1F, G). Under constant chemical gradients, it took 10 ~ 30 sec for sGC to re-localize to the pseudopod once the localization disappeared, which is consistent with the refractory periods seen for sGC responses to pulse stimuli (Fig. 3A). These results suggest that the refractory period for the localization of a signaling molecule corresponds to the frequency of the pseudopod formation. This idea was further supported from observations that showed modulation of the intracellular cGMP concentration affected the refractory period in sGC responses and pseudopod formation. *gbpAΔ* cells lacking cGMP degradation activity showed prolonged refractoriness and prolonged suppression of F-actin polymerization and pseudopod formation (Fig. 5B, C, S4A) (Roelofs et al., 2001; Meima et al., 2002). The prolonged refractoriness has been reported also in *gbpAΔ* cells as a light-scattering response or  $\text{Ca}^{2+}$  influx upon a cAMP stimulus (Lusche and Malchow, 2005). Furthermore, *gcΔ* and *gbpCΔ* cells showed pseudopod formation more frequently than wild-type cells (Fig. 5C, 5D and Movie 4).

It has been reported that when stimulated twice at 30 sec intervals, cells synthesized cGMP upon the first stimulus but not upon the second, indicating some form of adaptation (Van Haastert and Van Der Heijden, 1983). That same report showed that the addition of a cAMP phosphodiesterase enabled cGMP production in response to both stimuli. These results suggest that cGMP could be produced repetitively when cAMP stimulation is short enough so

as to avoid complete adaptation. Our optical-uncaging experiment was likely to have provided a transient stimulus to the cells before adaptation occurred, although the intracellular cGMP levels were not measured. Based on these observations, we suggest that the refractory period regulated by cGMP-dependent GbpC signaling is a physiologically important feature for chemotactic cell migration.

Although cAMP stimulus induces PIP3 and sGC excitation on the membrane independently (Fig. S1G, H), there may be crosstalk between these pathways. We showed that sGC localization strongly depends on F-actin dynamics (Fig. 2C). Previous studies showed that F-actin is required for PI3K localization to the pseudopod and thereby positive feedback comprising Ras, PI3K and F-actin is important for directional cell migration (Sasaki et al., 2004). These observations suggest positive feedback between the PI3K-PTEN and sGC pathways through F-actin dynamics. This crosstalk could control pseudopod dynamics positively and cooperatively. We further found that pseudopods have different molecular fingerprints, in which most pseudopods show sGC localization but only half show both sGC and PIP3 localization (Fig. 1B). Thus, these two types of pseudopods differ. The localization of both sGC and PIP3 extends pseudopods more extensively than the localization of either alone (Fig. 1E). Additionally, the life-times and contribution to cell movement are longer and bigger (Fig. S1C, D). Thus, these parallel pathways regulate the pseudopod elongation additively.

Our results are summarized as a scheme (Fig. 5E). Chemoattractant stimulations trigger sGC translocation to F-actin on the membrane (Fig. 2C, D). At the same time, sGC catalyzes cGMP production upon chemoattractant stimulation (Roelofs and Van Haastert, 2002). Increased cGMP binds to GbpC directly and induces its kinase activation through a series of intramolecular signals. Then it initiates the destabilization of F-actin and in turn suppresses further pseudopod elongation and induces pseudopod retraction (Fig. 5C). In our scheme, cGMP-dependent GbpC signaling defines the refractoriness in sGC excitability, which is linked to suppression of the pseudopod. It has been previously reported that GbpC provides major intracellular cGMP binding sites at a high affinity of  $K_d = \text{around } 10^{-9} \text{ M}$  and slow dissociation rate with a half-life of  $\sim 2 \text{ min}$  (Van Haastert et al., 1982). These kinetics disagree with our model, which assumes a much faster dissociation for cGMP of 20-30 sec. To resolve this discrepancy, an unknown factor with low affinity and fast dissociation to cGMP could function downstream of cGMP bound GbpC or a threshold must be passed for cGMP-bound GbpC to disrupt F-actin stability. Future work will clarify how cGMP regulates F-actin suppression through GbpC.

Previous studies have also shown that cGMP and GbpC signaling activation induces pseudopod suppression at the rear end of cells via the regulation of myosin II (Bosgraaf et al., 2005; Veltman and Van Haastert, 2007). On the other hand, it is known that myosin II is not

essential for the retraction of the anterior pseudopod observed in *mhcAΔ* cells (Iwadate and Yumura, 2008). We found myosin II was not essential for sGC excitation upon cAMP stimulation (Fig. 4C). Taken together, cGMP-dependent GbpC signaling could serve for anterior retraction of the pseudopod, with myosin II making only a minor contribution.

cGMP-dependent GbpC signaling constitutes delayed negative feedback in the sGC excitable pathway, which provides a mechanism underlying the fast cycling of repeated pseudopod formation via shortening of the refractory period. Multiple signaling pathways with different refractory periods can regulate pseudopods at different time scales for chemotaxis. Such pseudopod regulation mechanisms may provide flexibility for motile cells to respond to complex environmental stimulations at various time scales.

## Materials & Methods

### Cell Preparation and Plasmids

*Dictyostelium discoideum* cells were grown at 22 °C in HL5 medium supplemented with 6 ng/ml Vitamin B12 and 100 ng/ml folic acid (Watts and Ashworth, 1970). Wild-type AX2 and AX3 cells were used in this study. The AX2 cell line was used for simultaneous imaging of sGC<sub>N</sub>-Halo and PH<sub>PKB</sub>-GFP, sGC-GFP and mRFP-LimEΔcoil. Because *pi3k1Δ2Δ* and *arcB* mutant cells were derived from the AX2 cell line, sGC-GFP responses in these strains were compared to AX2 cells. AX3 cells were used as controls when observing sGC-GFP and mRFP-LimEΔcoil localization, because the mutant strains *gcaΔ* (*sgcΔ/gcaΔ*), *gbpAΔ*, *gbpAΔ*, *gbpCΔ*, *gbpDΔ* and *mhcAΔ* were derived from the AX3 cell line. All plasmids and strains are listed in supplementary Tables 1, 2. When grown with selection, medium was supplemented with 10 μg/ml blasticidin S, 20 μg/ml G-418, or 50 μg/ml hygromycin B. Cells were starved for 5~7 h in development buffer consisting of 10 mM Na/K PO<sub>4</sub> (pH 6.5), 2 mM MgSO<sub>4</sub>, and 0.2 mM CaCl<sub>2</sub>. For cAMP stimulation experiments, cells were treated with 4 mM caffeine for 30 min to inhibit *de novo* adenylyl cyclase activity and deplete extracellular cAMP. Cells were placed on glass-bottom dishes (IWAKI). *sgcΔ* cells were generated from AX2 by homologous recombination using a disruption cassette containing the blasticidin S resistance (BSR) gene. Two regions of the *sgc* sequence, from 607 to 1116 and 4194 to 4891, were amplified by using the full-length *sgc* gene as a template, and the BSR gene was inserted between them. The construct was linearized with *Bam*HI and introduced into AX2 and *sgcΔ* cells, which were selected with 10 μg/ml blasticidin S. The cloned transformants were screened by PCR of their isolated genomic DNAs. The N-terminal fragment of sGC (sGC<sub>N</sub>, amino acids 1-1019) and N-terminal deletion fragment (sGCΔN, amino acids 877-2843) were amplified by PCR and cloned into pHK12-Halo7 to yield C-terminal Halo7 tagged proteins.

The full-length *gfpA* gene was amplified by PCR and cloned into pDM358-eGFP to yield C-terminal eGFP tagged protein.

### **Fluorescence Imaging and Pulse cAMP Stimulation**

Fluorescence images were obtained by using a confocal microscope (FV1000, Olympus) with a 60×/1.35 NA oil immersion objective lens and software (Fluoview, Olympus). TMR and mRFP were excited by a 543 nm He-Ne laser, and GFP was excited by a 488 nm Ar laser. For pulse cAMP stimulation, cells were placed on a 4-cm round cover glass (Matsunami) with a flow chamber (FCS2, Bioptics). The inlet of the chamber was connected to a 10-ml glass syringe (Top) mounted in the syringe pumps (FP-1000, Melquest). The syringe was filled with development buffer containing 4 mM caffeine and 5 nM DEACM-caged cAMP (Biolog). Photolytic activation of caged cAMP by a 405 nm Mercury lamp was carried out upstream of the cells, and activated cAMP was flowed out. To demonstrate the temporal change of cAMP concentration, 100  $\mu$ M CMNB-caged fluorescein (Invitrogen) was used instead of caged cAMP (Fig. S2B). The flow rate was 300  $\mu$ l/min. In repetitive pulse stimulus experiments, all exposures were carried out by 1.5 sec laser irradiation. To align the first pulse timing, data were normalized by the maximum value of cytosolic fluorescence intensity.

### **Pseudopod Characterization and Cell Motility Assay**

Differentiated cells without caffeine treatment were put on a glass bottom dish and captured by the confocal microscope at 5 sec intervals for at least 5 min. The pseudopod dynamics was analyzed by ImageJ according to the localization patterns of sGC and PIP3. The positions of the sGC and PIP3 signals were assigned from the fluorescence images to distinguish two types of localization: sGC alone and the co-localization of sGC and PIP3. Morphological changes were extracted by differentiating between two consecutive binarized fluorescence images. In this study, we defined a pseudopod as an area that extended beyond 4  $\mu$ m<sup>2</sup>/frame during growth. These extracted pseudopods were characterized by quantifying the size, the appearance frequency, the life-time, and the contribution to cell movement. The size was defined by the elongation length between the beginning and end points of a pseudopod during its total life cycle. The appearance frequency, or the average number of pseudopods per cell, was calculated by dividing the total number of pseudopods on each cell by the recorded time. The life-time is the length of time in which a positive change was maintained in each pseudopod's area. The contribution to cell movement was defined as the displacement of the centroid of a pseudopod during its life-time. For cell motility analysis, developed cells without caffeine treatment were observed with an Olympus IX-71 inverted microscope capable of producing phase contrast optics. Movie files were recorded with a CCD camera (Digital Sight, Nikon) and software (NIS-Elements, Nikon). Cell behavior was recorded for



20 min at 5-sec intervals, and images were analyzed using laboratory-developed software. The motility speed of each cell was calculated as the average speed for each short trajectory.

### **sGC Domain Analysis on the Cell Membrane**

Membrane localization of sGC-GFP was analyzed by ImageJ. The fluorescence intensity profile of sGC-GFP on the membrane was obtained at every pixel along the cell periphery and processed with a 15 pixels moving average. In order to compensate for different sGC-GFP expression levels, profiles were normalized by the membrane fluorescence intensity in the absence of sGC localization. To compare sGC localization under various conditions, we defined localization amplitude and domain size as follows. Localization amplitude represents the maximum value of the normalized intensity along the cell membrane. Domain size was quantified as the ratio of the region with the normalized value exceeding the threshold to the overall membrane area. The threshold was set as 1.2 in this report.

### **Kymograph Analysis**

The spatiotemporal dynamics of fluorescence probes on cell membranes was analyzed and shown as 2D patterns by ImageJ. To monitor the pseudopod dynamics of moving cells, kymographs of the mRFP-LimE $\Delta$ coil localization in Fig. 5C were generated using an ImageJ plugin. The second response time was defined as the time that a cell showed mRFP-LimE $\Delta$ coil localization after its first response to 10 nM cAMP. Some cell lines showed a persistent response without transient suppression. The second response time of those cells was counted as 0. sGC<sub>N</sub>-TMR and PH<sub>PKB</sub>-GFP localizations on the bottom surface of the cell in Fig. 1C, D were analyzed by the reslice function in ImageJ after 1.0 pixel mean filtering of movie.

### **Cytoskeletal Actin Assay**

As previously described (Kamimura et al., 2016), differentiated cells were incubated in phosphate magnesium buffer (2 mM MgSO<sub>4</sub> in 5 mM Na/KPO<sub>4</sub> buffer, pH 6.5) with 3 mM caffeine at  $3 \times 10^7$  cells/ml. The cell suspension was stimulated with cAMP at a final concentration of 10 nM. After stimulation, cells were lysed by adding equal volumes of 2 $\times$  assay buffer consisting of 2% Triton X-100, 20 mM KCl, 20 mM EGTA, 20 mM imidazole and 0.1 mg/ml NaN<sub>3</sub>, and incubated on ice for 10 min. The samples were centrifuged at 8,000  $\times$ g for 4 min to collect the pellet fraction followed by washing with 1 $\times$  assay buffer and boiled in 2 $\times$  SDS sample buffer. Finally, the samples were analyzed by PAGE and stained with Coomassie Brilliant Blue. Images were acquired with ImageQuant LAS4000 for the quantification of actin (40 kDa).



## Acknowledgements

We thank P. Van Haastert for the plasmids expressing sGC-GFP, sGC  $\Delta$  cat-GFP, and GbpC mutants, and National BioResource Project (NBRP)-Nenkin for the AX3, *gbpAA*, *gbpABA*, *gbpCA*, *gbpDA*, *mhcAA* and *mutated arcB* cells. We appreciate the basic information from DictyBase. We also thank Peter Karagiannis for critically reading the manuscript, and thank all members of the Ueda laboratory for discussions and technical assistance.

## Funding

This work was supported by Japan Society for the Promotion of Science (JSPS) KAKENHI Grant Number 15J01805 (to Y.T.), and partially supported by JSPS KAKENHI Grant Number 17K07396 (to Y.K.), and by the Advanced Research and Development Programs for Medical Innovation (AMED-CREST) JP17gm0910001 (to M.U.).

## References

- Arai, Y., Shibata, T., Matsuoka, S., Sato, M. J., Yanagida, T. and Ueda, M.** (2010). Self-organization of the phosphatidylinositol lipids signaling system for random cell migration. *Proc. Natl. Acad. Sci. USA.* **107**, 12399-12404
- Artemenko, Y., Lampert, T. J. and Devreotes, P. N.** (2014). Moving towards a paradigm: Common mechanism of chemotactic signaling in *Dictyostelium* and mammalian leukocytes. *Cell Mol. Life Sci.* **71**, 3711-3747
- Asano, Y., Nagasaki, A. and Uyeda, T. Q. P.** (2008). Correlated waves of actin filaments and PIP3 in *Dictyostelium* cells. *Cell Motil. Cytoskeleton* **65**, 923-934
- Beta, C., Wyatt, D., Rappel, W. J. and Bodenschatz, E.** (2007). Flow photolysis of spatiotemporal stimulation of single cells. *Anal. Chem.* **79**, 3940-3944
- Bosgraaf, L., Russcher, H., Smith, J. L., Wessels, D., Soll, D. R. and Van Haastert, P. J. M.** (2002). A novel cGMP signaling pathway mediating myosin phosphorylation and chemotaxis in *Dictyostelium*. *EMBO J.* **21**, 4560-4570
- Bosgraaf, L., Waijer, A., Engel, R., Visser, A. J. W. G., Wessels, D., Soll, D. and Van Haastert, P. J. M.** (2005). RasGEF-containing proteins GbpC and GbpD have differential effects on cell polarity and chemotaxis in *Dictyostelium*. *J. Cell Sci.* **118**, 1899-1910
- Bosgraaf, L. and Van Haastert, P. J. M.** (2009). Navigation of chemotactic cells by parallel signaling to pseudopod persistence and orientation. *PLoS ONE* **4**, e6842
- Cai, H. and Devreotes, P. N.** (2011). Moving in the right direction: How eukaryotic cells migrate along chemical gradients. *Semin. Cell Dev. Biol.* **22**, 834-841
- Cao, Y., Lopatkin, A. and You, L.** (2016). Elements of biological oscillations in time and space. *Nat. Struct. Mol. Biol.* **23**, 1030-1034
- Devreotes, P. N., Bhattacharya, S., Edwards, M., Iglesias, P. A., Lampert, T. and Miao, Y.** (2017). Excitable signal transduction networks in directed cell migration. *Annu. Rev. Cell Dev. Biol.* **33**, 103-125
- Fischer, M., Haase, I., Simmeth, E., Gerisch, G. and Muller-Taubenberger, A.** (2004). A brilliant monomeric red fluorescent protein to visualize cytoskeleton dynamics in *Dictyostelium*. *FEBS Lett.* **577**, 227-232
- Gerisch, G., Ecke, M., Wischnewski, D. and Schroth-Diez, B.** (2011). Different modes of state transitions determine pattern in the phosphatidylinositide-actin system. *BMC Biol.* **12**, 42
- Gerisch, G., Schroth-Diez, B., Muller-Taubenberger, A. and Ecke, M.** (2012). PIP3 waves and PTEN dynamics in the emergence of cell polarity. *Biophys. J.* **103**, 1170-1178
- Goldberg, J. M., Bosgraaf, L., Van Haastert, P. J. M. and Smith, J. L.** (2002). Identification of four candidate cGMP targets in *Dictyostelium*. *Proc. Natl. Acad. Sci. USA.* **99**, 6749-6754
- Hind, L. E., Vincent, W. J. B. and Huttenlocher, A.** (2016). Leading from the back: the role

of the uropod in neutrophil polarization and migration. *Dev. Cell* **38**, 161-169

**Huang, C. H., Tang, M., Shi, C., Iglesias, P. A. and Devreotes, P. N.** (2013). An excitable signal integrator couples to an idling cytoskeletal oscillator to drive cell migration. *Nat. Cell Biol.* **15**, 1307-1316

**Iwadate, Y. and Yumura, S.** (2008). Actin-based propulsive forces and myosin-II-based contractile forces in migrating *Dictyostelium* cells. *J. Cell Sci.* **121**, 1314-1324

**Kalil, K. and Dent, E. W.** (2005). Touch and go: guidance cues signal to the growth cone cytoskeleton. *Curr. Opin. Neurobiol.* **15**, 521-526

**Kamimura, Y., Xiong, Y., Iglesias, P. A., Hoeller, O., Bolourani, P. and Devreotes, P. N.** (2008). PIP<sub>3</sub>-independent activation of TorC2 and PKB at the cell's leading edge mediates chemotaxis. *Curr. Biol.* **18**, 1034-1043

**Kamimura, Y., Miyanaga, Y. and Ueda, M.** (2016). Heterotrimeric G-protein shuttling via Gip1 extends the dynamic range of eukaryotic chemotaxis. *Proc. Natl. Acad. Sci. USA.* **113**, 4356-4361

**Khamviwath, V., Hu, J. and Othmer, H. G.** (2013). A continuum model of actin waves in *Dictyostelium discoideum*. *PLoS ONE* **8**, e64272

**Kortholt, A., Rehmann, H., Kae, H., Bosgraaf, L., Keizer-Gunnink, I., Weeks, G., Wittinghofer, A. and Van Haastert, P. J. M.** (2006). Characterization of the GbpD-activated Rap1 pathway regulating adhesion and cell polarity in *Dictyostelium discoideum*. *EMBO J.* **281**, 23367-23376

**Kortholt, A., Kataria, R., Keizer-Gunnink, I., Van Egmond, W. N., Khanna, A. and Van Haastert, P. J. M.** (2011). *Dictyostelium* chemotaxis: essential Ras activation and accessory signaling pathways for amplification. *EMBO Rep.* **12**, 1273-1279

**Kuwayama, H., Ishida, S. and Van Haastert, P. J. M.** (1993). Non-chemotactic *Dictyostelium discoideum* mutants with altered cGMP signal transduction. *J. Cell Biol.* **123**, 1453-1462

**Kuwayama, H., Viel, G. T., Ishida, S. and Van Haastert, P. J. M.** (1995). Abberant cGMP-binding activity in non-chemotactic *Dictyostelium discoideum* mutants. *Biochim. Biophys. Acta* **1268**, 214-220

**Langridge, P. D. and Kay R. R.** (2007). Mutants in the *Dictyostelium* Arp2/3 complex and chemoattractant-induced actin polymerization. *Exp. Cell Res.* **313**, 2563-2574

**Lusche, D. F. and Malchow, D.** (2005). Developmental control of cAMP-induced Ca<sup>2+</sup>-influx by cGMP: influx is delayed and reduced in a cGMP-phosphodiesterase D deficient mutant of *Dictyostelium discoideum*. *Cell Calcium* **37**, 57-67

**Mayor, R. and Etienne-Manneville, S.** (2016). The front and rear of collective cell migration. *Nat. Rev. Mol. Cell Biol.* **17**, 98-109

**Meili, R., Ellsworth, C., Lee, S., Reddy, T. B. K., Ma, H. and Firtel, R. A.** (1999). Chemoattractant-mediated transient activation and membrane localization of Akt/PKB is

required for efficient chemotaxis to cAMP in *Dictyostelium*. *EMBO J.* **18**, 2092-2105

**Meima, M. E., Biondi, R. M. and Schaap, P.** (2002). Identification of a novel type of cGMP phosphodiesterase that is defective in the chemotactic *stmF* mutants. *Mol. Biol. Cell* **13**, 3870-3877

**Nishikawa, M., Horning, M., Ueda, M., and Shibata, T.** (2014). Excitable signal transduction induces both spontaneous and directional cell asymmetries in the phosphatidylinositol lipid signaling system for eukaryotic chemotaxis. *Biophys. J.* **106**, 723-734

**Roelofs, J., Meima, M., Schaap, P and Van Haastert, P. J. M.** (2001). The *Dictyostelium* homologue of mammalian soluble adenylyl cyclase encodes a guanylyl cyclase. *EMBO. J.* **20**, 4341-4348

**Roelofs, J. and Van Haastert, P. J. M.** (2002). Characterization of two unusual guanylyl cyclases from *Dictyostelium*. *J. Biol. Chem.* **277**, 9167-9174

**Sager, B. M.** (1996). Propagation of traveling waves in excitable media. *Genes Dev.* **10**, 2237-2250

**Sasaki, A. T., Chun, C., Takeda, K. and Firtel, R. A.** (2004). Localized Ras signaling at the leading edge regulates PI3K, cell polarity, and directional cell movement. *J. Cell Biol.* **167**, 505-518

**Sato, M. J., Kuwayama, H., van Egmond, W. N., Takayama, A. L. K., Takagi, H., van Haastert, P. J. M., Yanagida, T., and Ueda, M.** (2009). Switching direction in electric-signal-induced cell migration by cyclic guanosine monophosphate and phosphatidylinositol signaling. *Proc. Natl. Acad. Sci. USA.* **106**, 6667-6672.

**Servant, G., Weiner, O. D., Herzmark, P., Balla, T., Sedat, J. W. and Bourne, H. R.** (2000). Polarization of chemoattractant receptor signaling during neutrophil chemotaxis. *Science* **287**, 1037-1040

**Shibata, T., Nishikawa, M., Matsuoka, S. and Ueda, M.** (2013). Intracellular encoding of spatiotemporal guidance cues in a self-organizing signaling system for chemotaxis in *Dictyostelium* cells. *Biophys. J.* **105**, 2199-2209

**Soll, D. R., Wessels, D., Kuhl, S. and Lusche, D. F.** (2009). How a cell crawls and the role of cortical myosin II. *Eukaryot. Cell* **8**, 1381-1396

**Tang, M., Wang, M., Shi, C., Iglesias, P. A., Devreotes, P. N. and Huang, C. H.** (2014). Evolutionarily conserved coupling of adaptive and excitable networks mediates eukaryotic chemotaxis. *Nat. Commun.* **5**, 5175

**Van Egmond, W. N., Kortholt, A., Plak, K., Bosgraaf, L., Bosgraaf, S., Keizer-Gunnink, I. and**

**Van Haastert, P. J. M.** (2008). Intramolecular activation mechanism of the *Dictyostelium* LRRK2 homolog Roco protein GbpC. *J. Biol. Chem.* **283**, 30412-30420

**Van Haastert, P. J. M., Van Walsum, H., and Pasveer, F. J.** (1982). Nonequilibrium

kinetics of a cyclic GMP-binding protein in *Dictyostelium discoideum*. *J. Cell Biol.* **94**, 271-278

**Van Haastert, P. J. M., and Van Der Heijden.** (1983). Excitation, adaptation, and deadaptation of the cAMP-mediated cGMP response in *Dictyostelium discoideum*. *J. Cell Biol.* **96**, 347-353

**Van Haastert, P. J. M. and Devreotes, P. N.** (2004). Chemotaxis: signaling the way forward. *Nat. Rev. Mol. Biol. Cell* **5**, 626-634

**Veltman, D. M., Roelofs, J., Engel, R., Visser, A. J. and Van Haastert, P. J. M.** (2005). Activation of soluble guanylyl cyclase at the leading edge during *Dictyostelium* chemotaxis. *Mol. Biol. Cell* **16**, 976-983

**Veltman, D. M. and Van Haastert, P. J. M.** (2006). Guanylyl cyclase protein and cGMP product independently control front and back of chemotaxing *Dictyostelium* cells. *Mol. Biol. Cell* **17**, 3921-3929

**Veltman, D.M. and Van Haastert, P. J. M.** (2007). The role of cGMP and the rear of the cell in *Dictyostelium* chemotaxis and cell streaming. *J. Cell Sci.* **121**, 120-127

**Veltman, D. M., Keizer-Gunnik, I. and Van Haastert, P. J. M.** (2008). Four key signaling pathways mediating chemotaxis in *Dictyostelium discoideum*. *J. Cell Biol.* **180**, 747-753

**Watts, D.J. and Ashworth, J. M.** (1970). Growth of myxamoebae of the cellular slime mould *Dictyostelium discoideum* in axenic culture. *Biochem. J.* **119**, 171-174

**Xiong, Y., Huang, C. H., Iglesias, P. A. and Devreotes, P. N.** (2010). Cells navigate with a local-excitation, global-inhibition-biased excitable network. *Proc. Natl Acad. Sci. USA* **107**, 17079-17086

## Figures

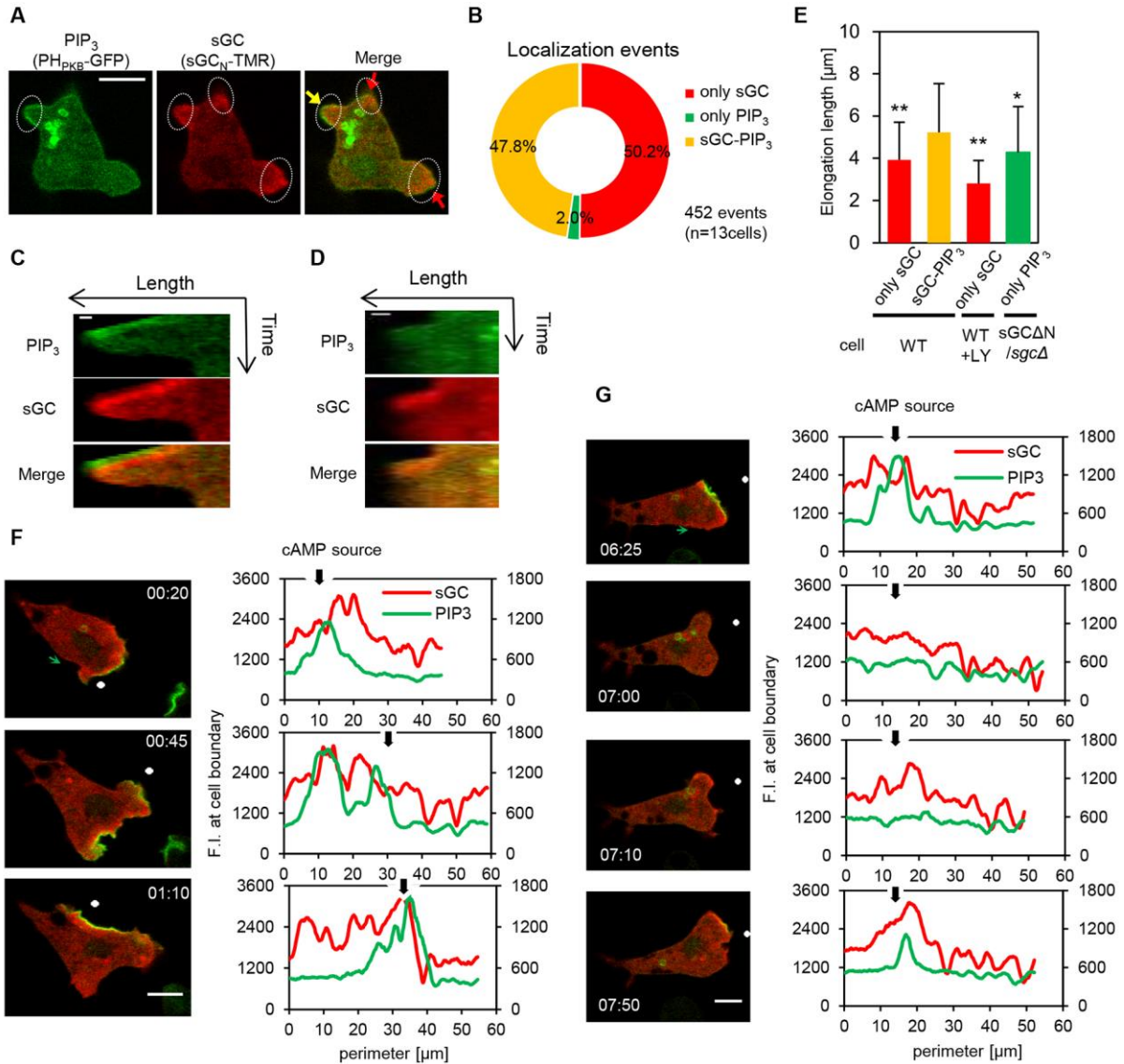


**Fig. 1. Simultaneous imaging of sGC and PIP3 localizations to the membrane**

(A) Representative pseudopods with sGC localization alone (red arrow) or sGC and PIP3 co-localization (yellow arrow) are shown by dotted circles. sGC and PIP3 in a wild-type AX2 cell were visualized by expressing sGC<sub>N</sub>-TMR and PH<sub>PKB</sub>-GFP, respectively. (Scale bar, 5  $\mu$ m) (B) Fraction of pseudopods with sGC, PIP3, or both sGC and PIP3 localization were quantified and are shown by the pie chart. (C and D) The temporal dynamics of sGC<sub>N</sub>-TMR and PH<sub>PKB</sub>-GFP during pseudopod elongation are shown by kymographs. Bottom surface of a

cell was observed by confocal microscopy at 5-sec intervals. Pseudopod elongation with localization of sGC<sub>N</sub>-TMR and PH<sub>PKB</sub>-GFP (C) or sGC<sub>N</sub>-TMR alone (D) are shown. (Scale bars, 1 μm) (E) The elongation length of sGC localized or sGC and PIP3 co-localized pseudopods were measured in wild-type AX2 cells (left). sGC<sub>N</sub>-TMR localization in AX2 cells treated with 30 μM LY294002 (middle) and PH<sub>PKB</sub>-GFP localization in *sgcA* expressing sGCΔN-Halo (right) (mean + s.d. for at least 39 pseudopods; \* P < 0.05, \*\* P < 0.001 versus sGC-PIP3, Bonferroni test). Spontaneous migration of each cell was recorded for 5-10 min. (F and G) The temporal responsiveness of sGC<sub>N</sub>-TMR and PH<sub>PKB</sub>-GFP to a cAMP gradient. The position of the pipette containing 40 nM cAMP is shown by a white dot in the pictures and black arrows in the profiles. The pipette's position was moved in (F) and fixed in (G). Fluorescence intensity of sGC and PIP3 along the cell surface was measured starting from green arrows (the top pictures) in the cell images. Time format is “mm:ss” (Scale bars are 5 μm).



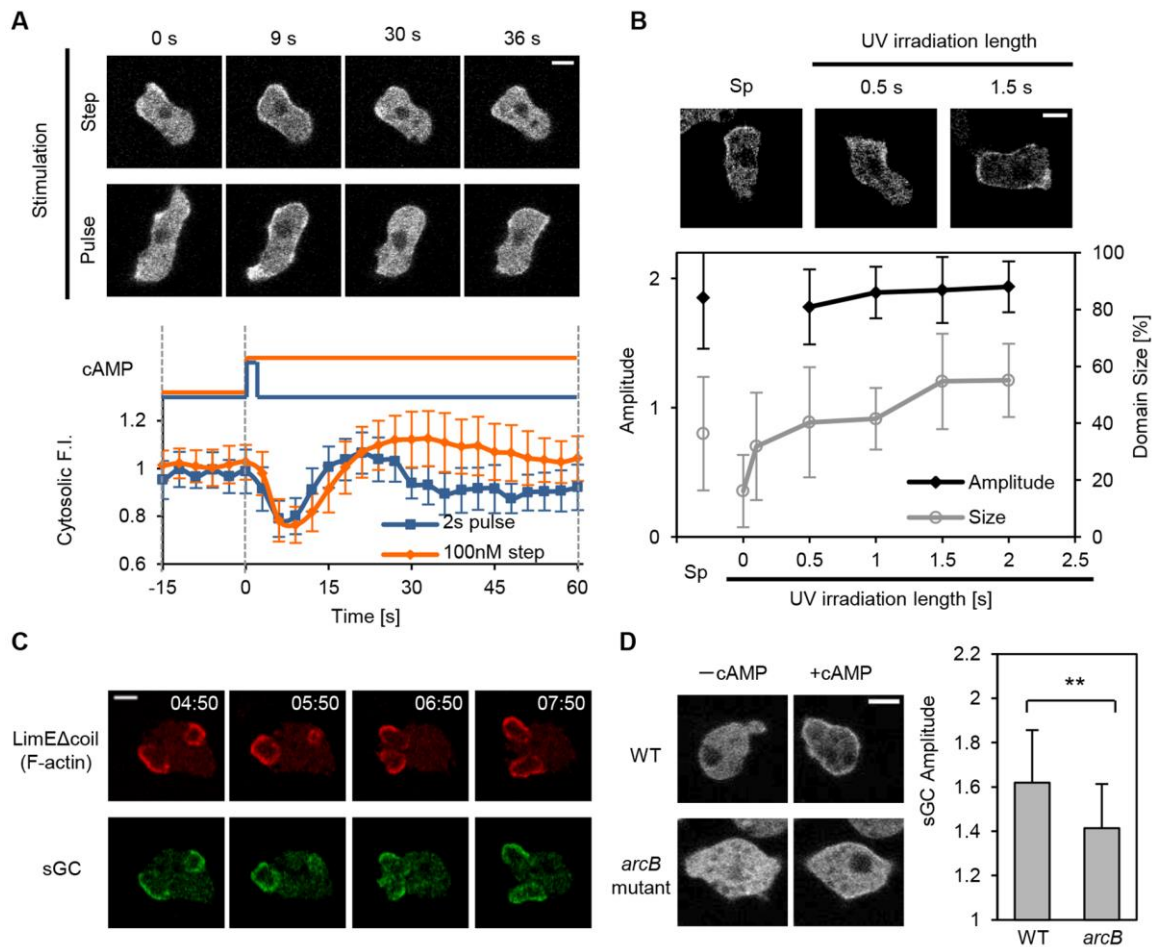


**Fig. 2. Excitable dynamics of sGC localization to the membrane**

(A) A *gcΔ* cell expressing sGC-GFP was stimulated upon pulse and step inputs of cAMP. Representative images at the indicated times after a 100-nM step (top row) or 2-sec pulse (bottom row) stimulus are shown. The bottom panel shows the comparison between sGC-GFP responses to pulse (blue) and step (orange) inputs. Responses (mean  $\pm$  s.d. for  $n = 12$  and  $24$  cells, respectively) of cytosolic sGC-GFP were normalized to the pre-stimulus level. (B) Excitable features of sGC-GFP localization were assessed by using UV-sensitive caged cAMP (see Materials and Methods). A *gcΔ* cell expressing sGC-GFP was stimulated upon various UV exposure times (top). Response amplitude and domain size of the sGC-enriched region are shown as functions of UV exposure time (bottom). Characteristics of the spontaneously formed domain are shown as Sp (mean  $\pm$  s.d. for at least 17 cells). (C) Co-localization pattern of F-actin and sGC. A wild-type AX2 cell co-expressing mRFP-LimEΔcoil and sGC-GFP was treated with  $1 \mu\text{M}$  LatA. The bottom of the cell was observed at 5-sec intervals. Time format is “mm:ss”. (D) Wild-type AX2 and *arcB* mutant cells expressing sGC-GFP were stimulated with 100 nM cAMP. Localization amplitude (mean  $\pm$  s.d. for  $n = 24$  and  $23$  cells, respectively) was quantified as in (B). (All scale bars are  $5 \mu\text{m}$ ; \*\*  $P < 0.001$ , t-test).

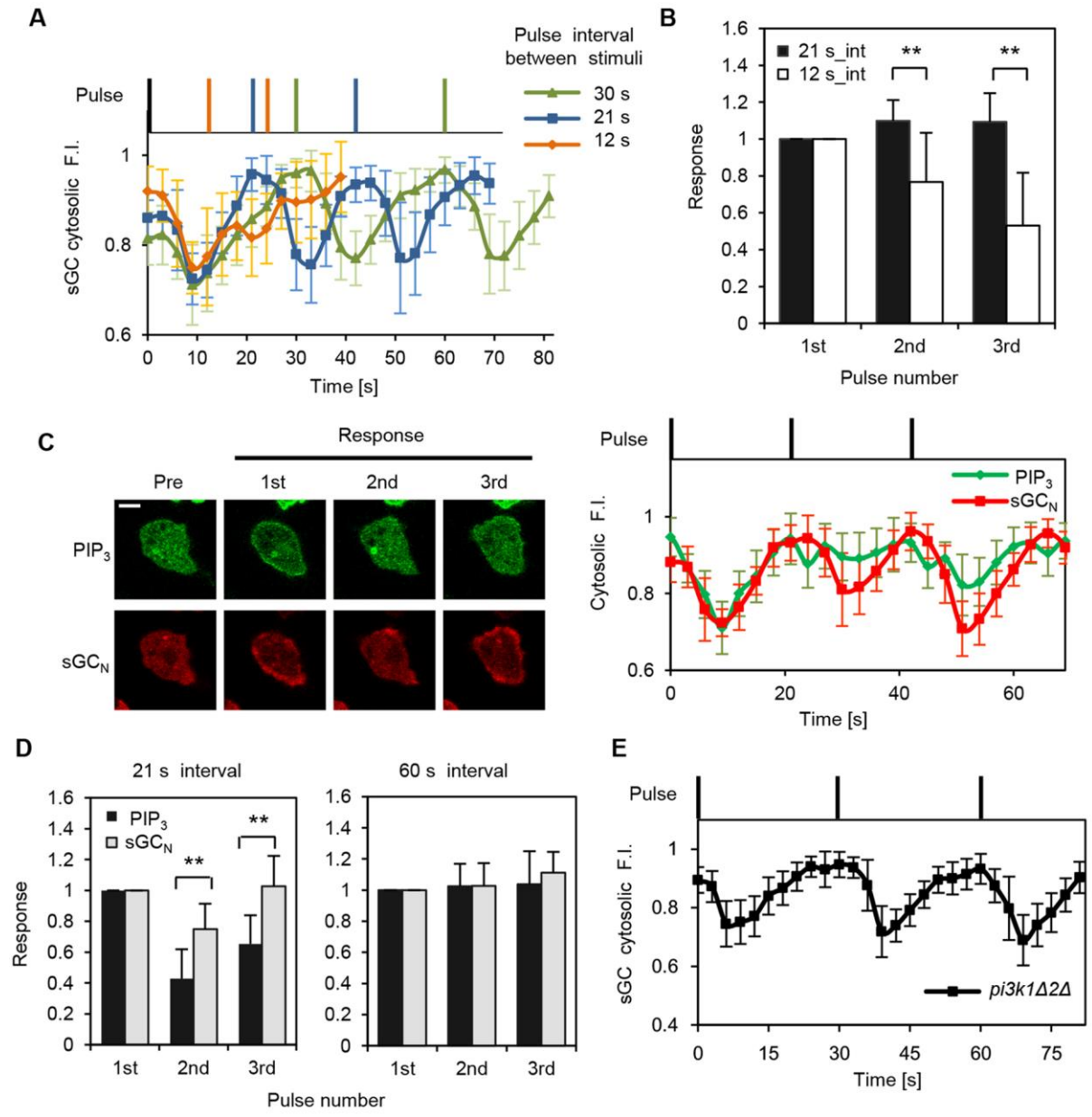


**Fig. 3. sGC-mediated signaling pathway has a shorter refractory period than PIP3-mediated pathway**

(A and B) Refractoriness of sGC-GFP requirement to the pseudopods. (A) A *gcΔ* cell expressing sGC-GFP was stimulated with 1.5 sec of pulsatile UV exposure three times. Cytosolic sGC-GFP responses to stimuli of various interval lengths were normalized by the maximum fluorescence value in the time course. Black and colour coded bars show the first stimulus timing and the pulse timing at different interval lengths, respectively. (B) Each cytosolic response of (A) was normalized to the value of the first response (mean + s.d. for at least 13 cells). (C and D) A wild-type AX2 cell co-expressing PH<sub>PKB</sub>-GFP and sGC<sub>N</sub>-TMR

was stimulated at 21-sec (C, D) or 60-sec (D) intervals by repetitive pulse stimuli. (C) Cytosolic responses to 21-sec interval stimuli were normalized by the maximum fluorescence value in the time course. Black bars on the abscissa represent the pulse timing. (D) Refractory responses of PH<sub>PKB</sub>-GFP and sGC<sub>N</sub>-TMR. Each cytosolic response to 21- or 60-sec interval stimuli was normalized by the value of the 1st response (mean + s.d. for n = 12 and 10 cells, respectively). (E) sGC-GFP responses to 30-sec interval stimuli in *pi3k1Δ2Δ* cells (mean ± s.d. for n = 16 cells) (Scale bar, 5 μm; \*\* P < 0.001, t-test).

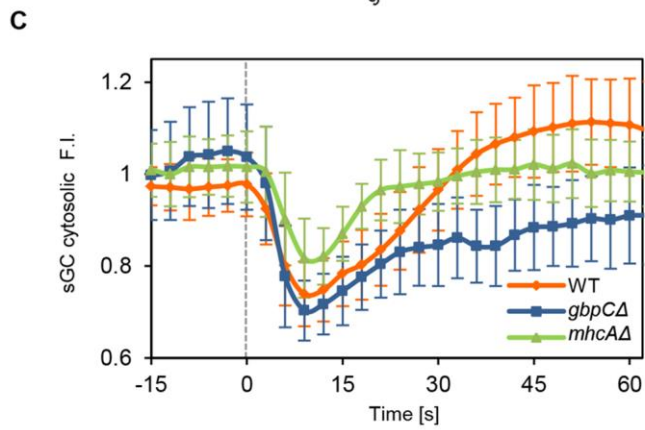
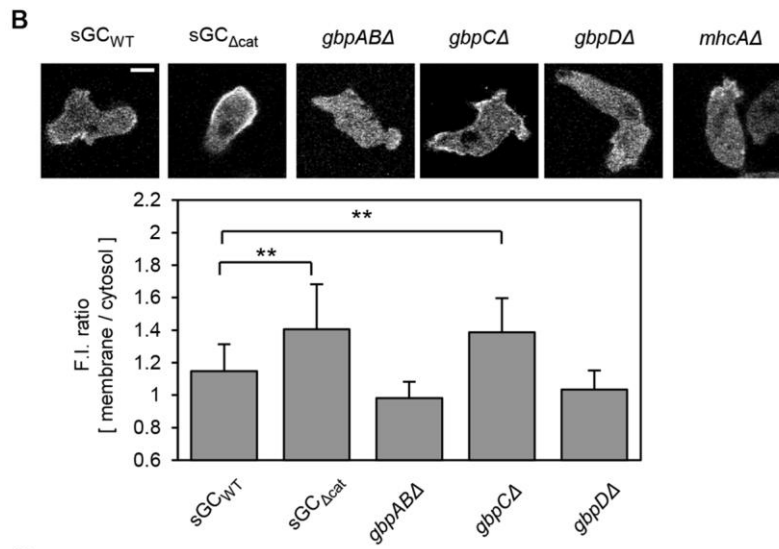
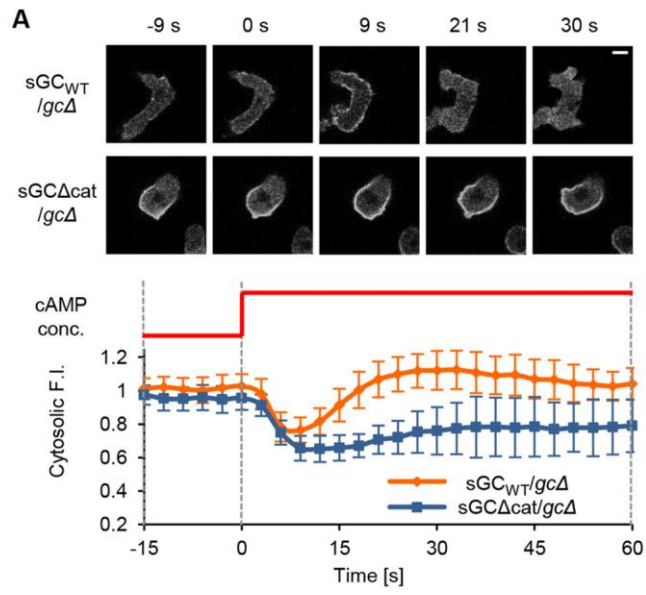


**Fig. 4. cGMP-GbpC signaling suppresses sGC localization upon cAMP stimulation.**

(A) *gcl* cells expressing sGC<sub>WT</sub>-GFP or sGC<sub>Δcat</sub>-GFP were stimulated with 100 nM cAMP. Representative images at the indicated times after cAMP stimulus are shown. The time courses of the cytosolic fluorescence intensity of sGC<sub>WT</sub> (the same data is shown in Figure 2A) and sGC<sub>Δcat</sub> are shown below (mean ± s.d. for n = 24 and 17 cells, respectively). (B) Pseudopod sGC localization in the indicated knockout cell lines (top). Fluorescence intensity ratio (mean + s.d. for at least 25 cells) between the plasma membrane and the cytosol without cAMP (bottom). (C) sGC responses of the indicated cell lines upon cAMP stimulation. Wild-type AX3 and mutant cells expressing sGC-GFP were stimulated with 100 nM cAMP. Cytosolic intensity was normalized to the pre-stimulus level (mean ± s.d. for at least n = 19 cells) (Scale bars, 5 μm; \*\* P < 0.001, t-test).

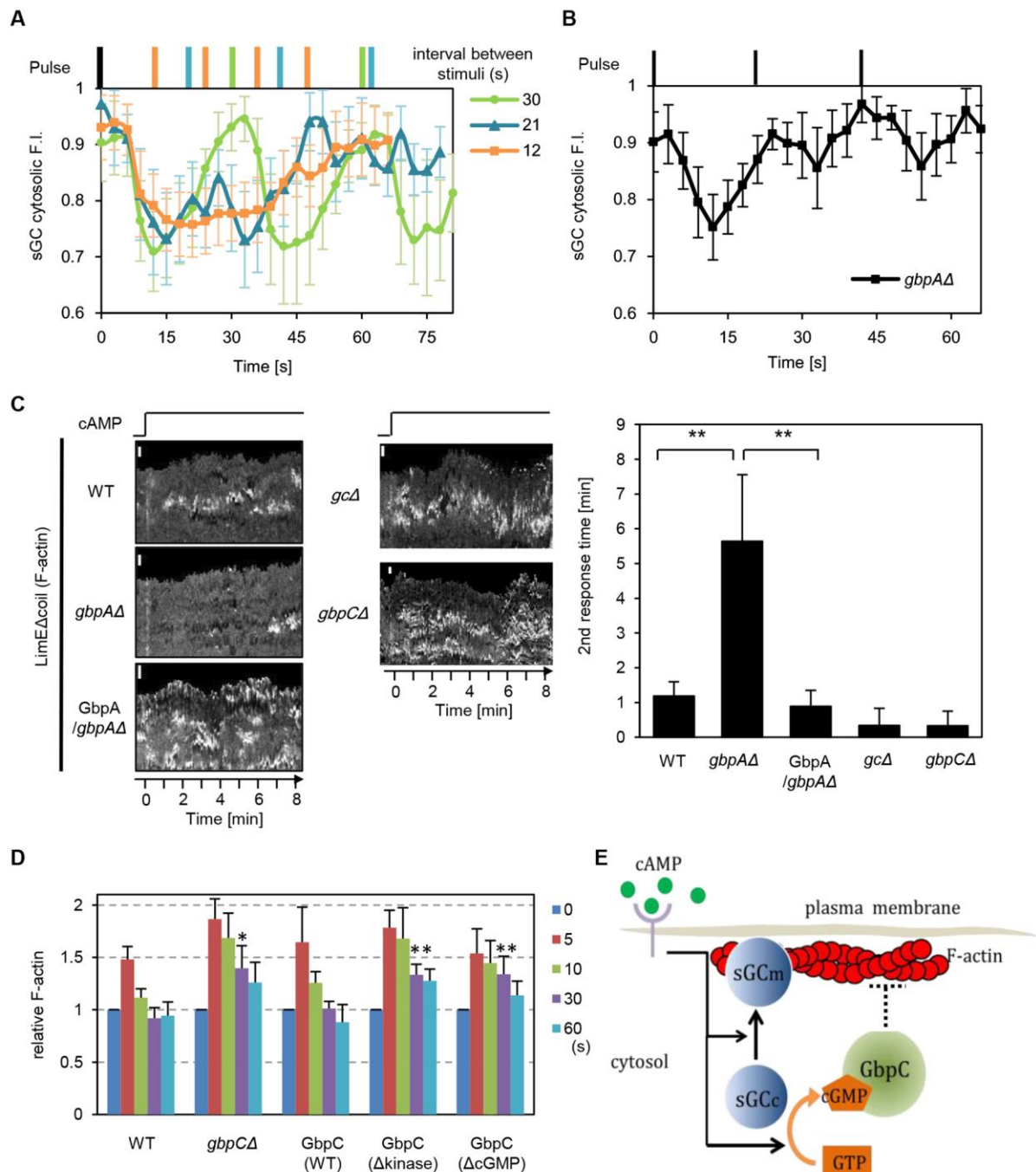


**Fig. 5. cGMP-GbpC signaling regulates the refractoriness of sGC responses.**

(A) Cytosolic sGC-GFP responses in *gbpCΔ* cells to repetitive stimuli. Colour coded bars represent pulse timing as shown in Fig. 3 (mean  $\pm$  s.d. for at least 11 cells). (B) Refractoriness of the sGC-GFP response depends on the amount of intracellular cGMP. *gbpAΔ* cells were repetitively stimulated with 21-sec interval pulses (mean  $\pm$  s.d. for  $n = 16$  cells). (C) Temporal dynamics of pseudopod formation upon a cAMP step stimulus. Kymographs of

wild-type AX3 and mutant cell lines were drawn by measuring the fluorescence intensity around the boundary of the cell expressing mRFP-LimE $\Delta$ coil (left). Scale bars, 5  $\mu$ m. Second response time represents the time required for secondary pseudopod formation after 10 nM cAMP stimulation at time 0 (right) (mean + s.d. for at least 40 cells; \*\* P < 0.001, t-test). (D) Cytoskeletal F-actin amounts upon 10 nM cAMP were normalized to the pre-stimulus level. GbpC (WT), GbpC ( $\Delta$ kinase) and GbpC ( $\Delta$ cGMP) represent *gbpC* $\Delta$  cells expressing wild-type, kinase dead and cGMP binding mutations of GbpC, respectively (mean + s.d. for at least 3 experiments; \* P < 0.05 versus wild-type, \*\* P < 0.05 versus GbpC (WT), t-test). (E) A schematic model of the sGC pathway in F-actin dynamics.



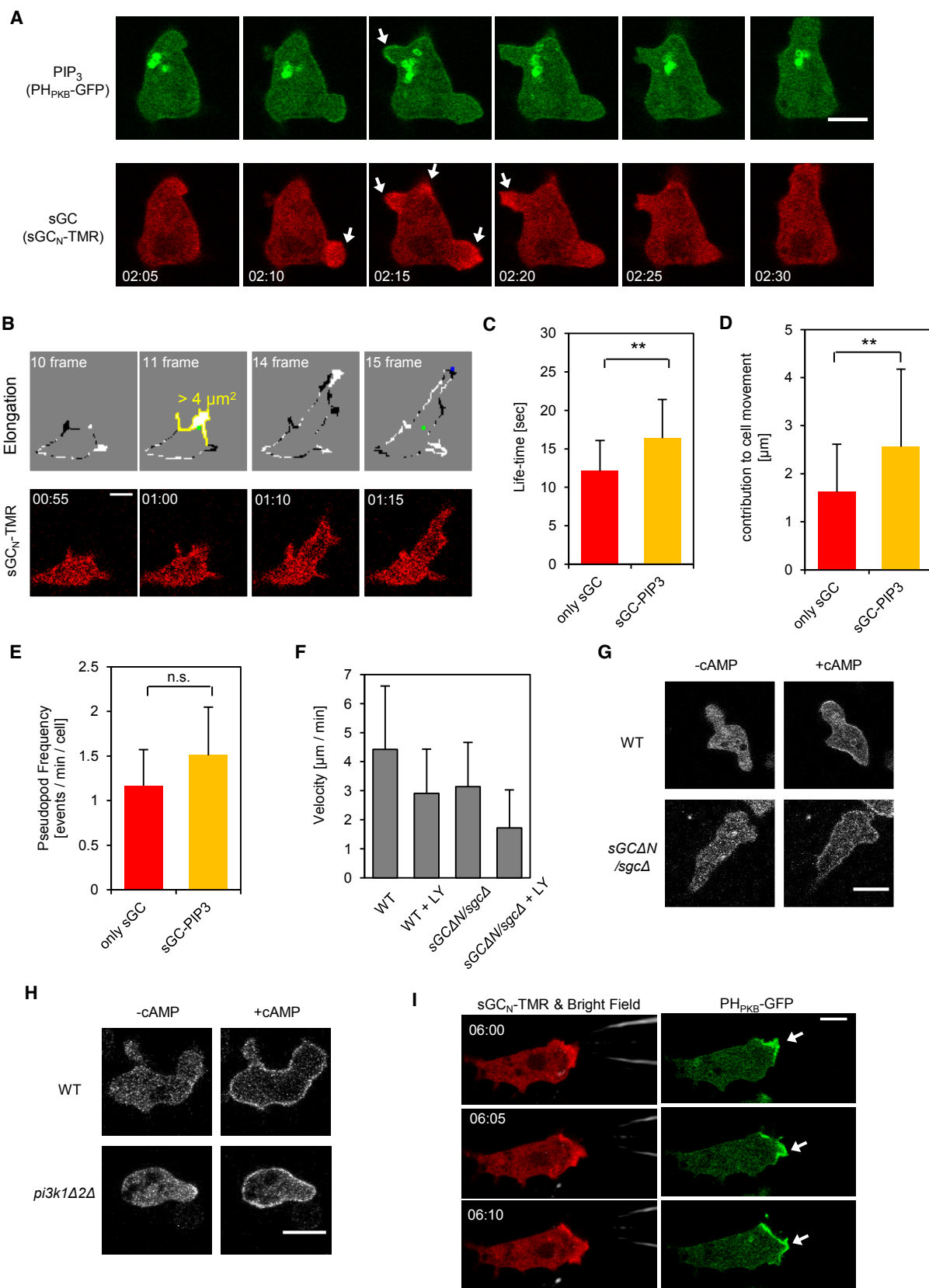


**Fig. S1. Independent function of parallel pathways**

(A) The time evolution of pseudopod dynamics shown in Figure 1A. sGC and PIP3 localizations are indicated by white arrows. (B) A representative pseudopod analysis. The fluorescence image of a cell with sGC<sub>N</sub>-TMR, shown in the bottom, was binarized and subtracted in two consecutive frames. The white and black colors in the upper panel show the positive and negative changes, respectively. An area more than 4  $\mu\text{m}^2$  (shown by the yellow ROI) was defined as a pseudopod and was pursued when it stopped expanding. The green and blue dots show the start and end points of the pseudopod, respectively. (C) The life-time of pseudopods with sGC alone or with the co-localization of sGC and PIP3 (mean + s.d. for n = 147 and 189 pseudopods, respectively). (D) Contribution to cell movement for pseudopods with sGC alone or with the co-localization of sGC and PIP3 (mean + s.d. for n = 147 and 189 pseudopods, respectively). (E) Frequencies of pseudopod formation with sGC alone or with the co-localization of sGC and PIP3. The number of pseudopods was counted if the elongation area was over 4  $\mu\text{m}^2$  (mean + s.d. for n = 13 cells). (F) Migration velocity of wild-type AX2 and *sgcA* cells expressing sGC $\Delta$ -Halo was analyzed in the presence or absence of 50  $\mu\text{M}$  LY294002 (see Methods). (G and H) PIP3 and sGC responses of the indicated cell lines at 1  $\mu\text{M}$  cAMP. PIP3 production of wild-type AX2 and sGC $\Delta$  / *sgcA* cells (G) and sGC localization of wild-type AX2 and *pi3k1A2A* cells (H) were observed by the expression of PH<sub>PKB</sub>-GFP and sGC-GFP, respectively. (I) Image galleries of a cell with sGC (red) and PIP3 (green) signals taken from supplementary Movie 1. The elongating pseudopod is shown by white arrows. Time format is “mm:ss”. Scale bars are 5 and 10  $\mu\text{m}$  in (A)-(C) and (H)-(I), respectively (\*\* P < 0.01, t-test).

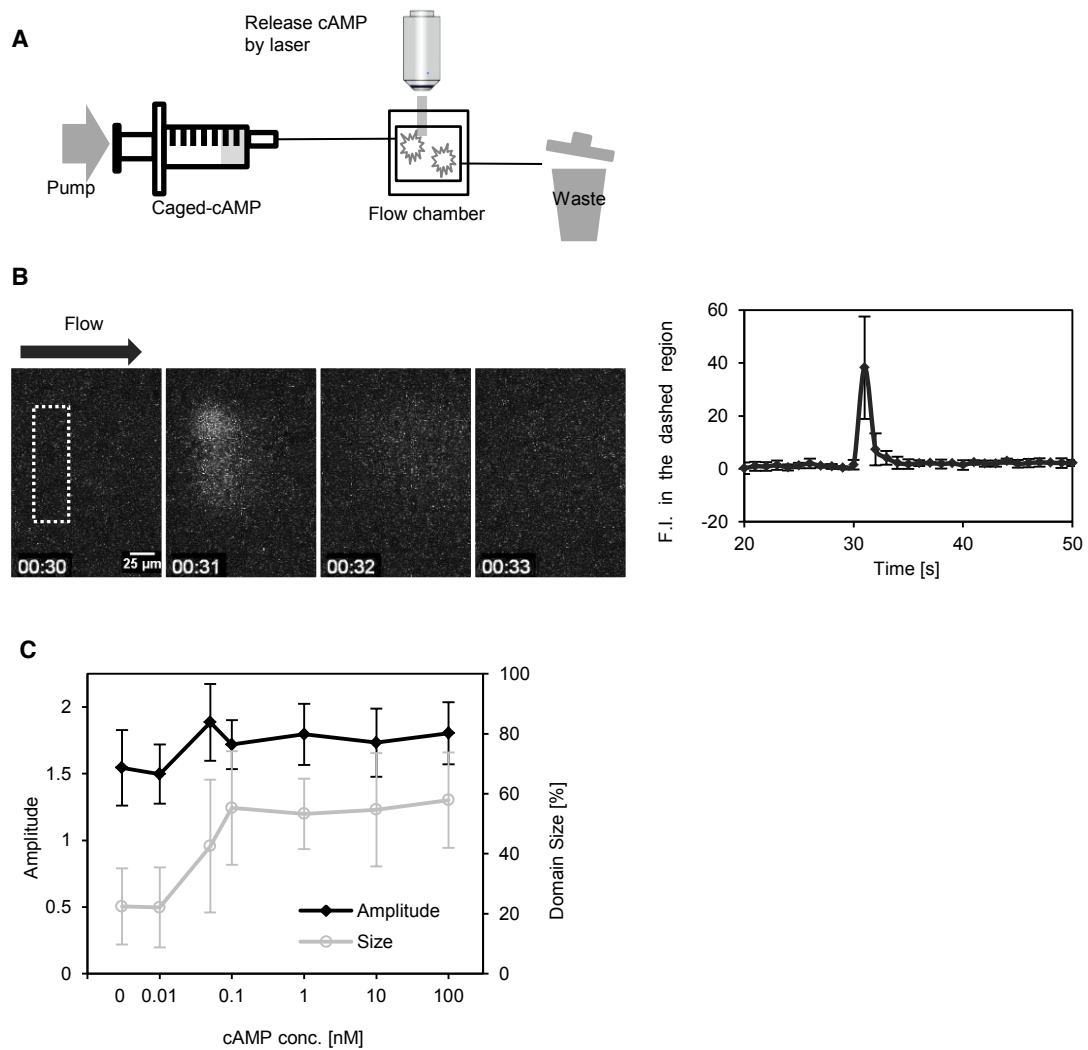


**Fig. S2. Construction of the cAMP pulse stimulation system**

(A) A schematic drawing of the pulse stimulation system. (B) Time course of the transient release of caged compound. Photolysis of 100 μM caged fluorescein in solution was carried out at the dashed region by UV flash (left). Fluorescence intensity of the region where UV was irradiated (right) (mean ± s.d. for n = 3). (C) *gcA* cells expressing sGC-GFP were stimulated with various cAMP concentrations. Response amplitude and domain size of the sGC-enriched region are shown as functions of cAMP concentrations. (mean ± s.d. for at least 8 cells).

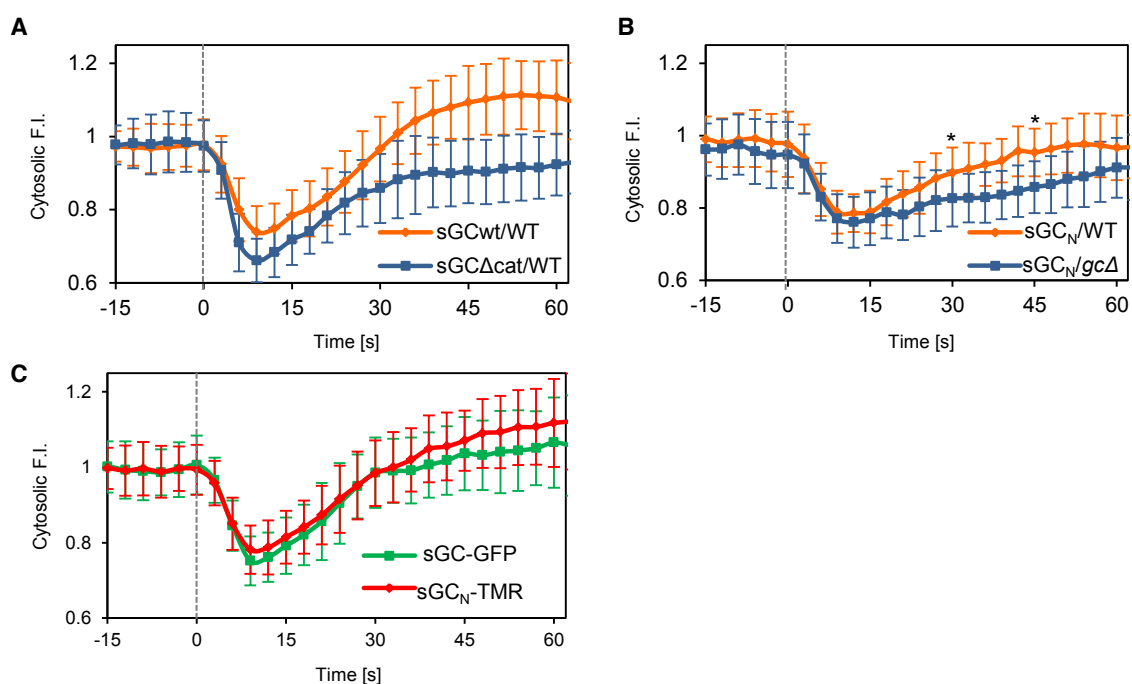


### Fig. S3. Evaluation of various sGC constructs

(A) sGC responses of the indicated cell lines upon cAMP stimulation. Wild-type AX3 cells expressing sGC<sub>WT</sub>-GFP or sGC $\Delta$ cat-GFP were stimulated with 100 nM cAMP. Cytosolic intensity was normalized to the pre-stimulus level (mean  $\pm$  s.d. for at least  $n = 19$  cells). For sGC<sub>WT</sub>-GFP, the same data is shown in Figure 4C. (B) The responses of the N terminus of sGC (sGC<sub>N</sub>) in wild-type or *gc* $\Delta$  cells were observed as in (A) (mean  $\pm$  s.d. for  $n = 29$  and  $28$  cells, respectively; \*  $P < 0.01$  versus wild-type cell at 30 and 45 sec, t-test). (C) The responses of the full-length (sGC) and the N-terminal sGC (sGC<sub>N</sub>) in the same wild-type cell were observed as in (A) (mean  $\pm$  s.d. for  $n = 19$  cells).

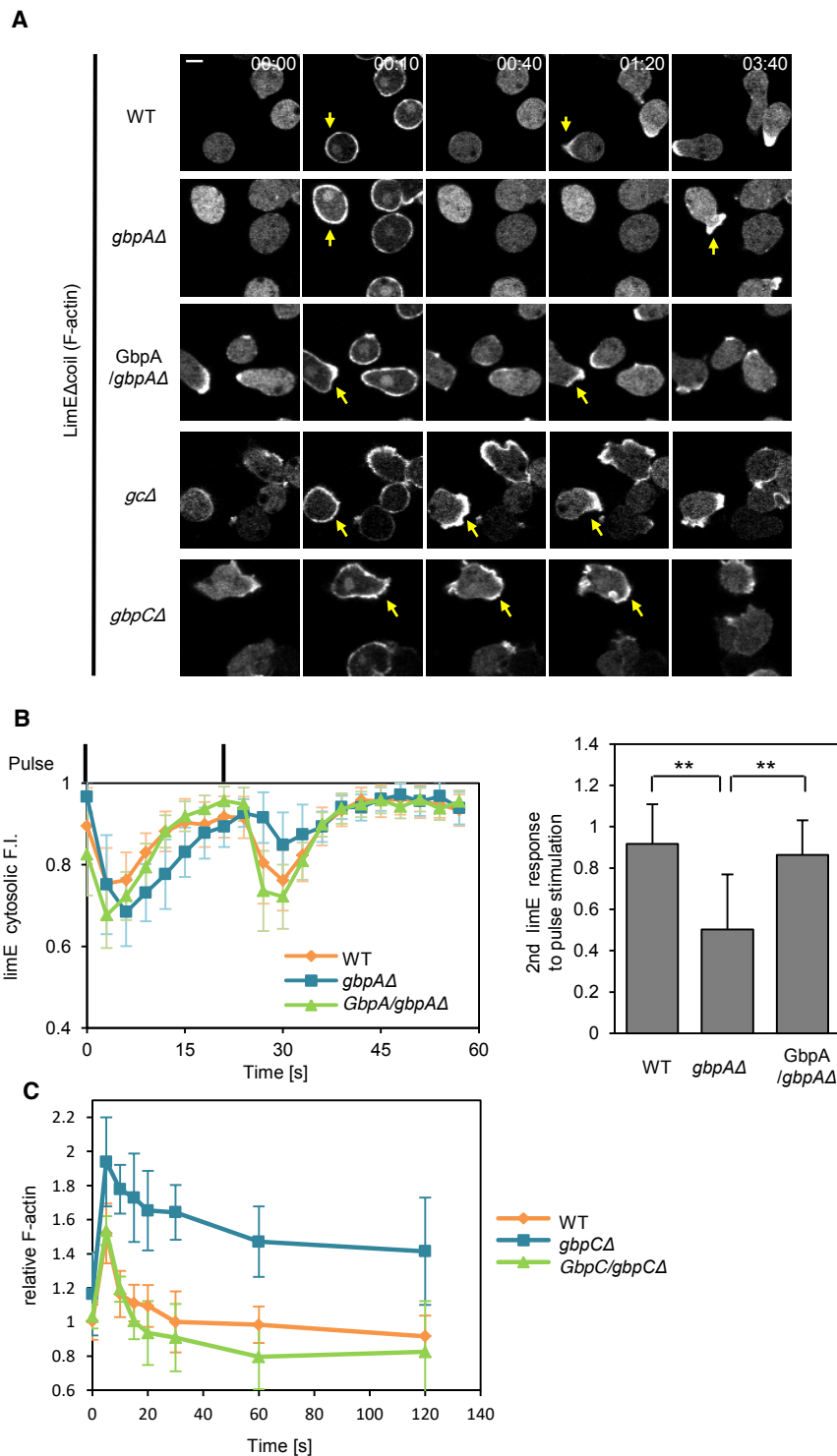


**Fig. S4. The recovery time of F-actin response depends on cGMP concentration**

(A) Wild-type AX3 and mutant cell lines expressing mRFP-LimE $\Delta$ coil were stimulated with 10 nM cAMP. Yellow arrows show the pseudopods where mRFP-LimE $\Delta$ coil localized. These pictures were clipped from Movies 3 and 4. (B) The refractoriness of F-actin depends on the amount of intracellular cGMP. Wild-type AX3, *gbpA* $\Delta$  and *gbpA* $\Delta$  rescued by GbpA cells expressing mRFP-LimE $\Delta$ coil were repetitively stimulated with 21-sec interval pulses (left) (mean  $\pm$  s.d. for  $n = 23$  cells). Cytosolic responses to 21-sec interval stimuli were normalized by the maximum fluorescence value in the time course. Black bars on the abscissa represent the pulse timing. The second responses normalized by the first responses of each cell line are shown (right) (mean + s.d.; \*\*  $P < 0.001$ , t-test). (C) Cytoskeletal F-actin amounts upon 10 nM cAMP shown in Figure 5D were normalized to the value of wild-type cells at 0 sec (mean  $\pm$  s.d. for at least 3 experiments).

**Table S1. Plasmid list.**

Plasmid name	Protein expressed	Tag	Backbone	Source or reference
sGC-GFP	SgcA	GFP	pMB74	Veltman et al., 2005
sGC $\Delta$ cat-GFP	SgcA(D1106A)	GFP	pMB74	Veltman et al., 2006
sGCN-Halo7	SgcA(1-1019)	Halo7	pHK12	this study
sGC $\Delta$ N-Halo7	SgcA(877-2843)	Halo7	pHK12	this study
PH <sub>PKB</sub> -eGFP	PkbA(1-113)	eGFP	pBIG	Meili et al., 1999
mRFP-LimE $\Delta$ coil	LimE(1-145)	mRFP	pHK12	this study
GbpA-eGFP	GbpA	eGFP	pDM358	this study

Numbers in parentheses refer to a mutation or regions of amino acid residues.

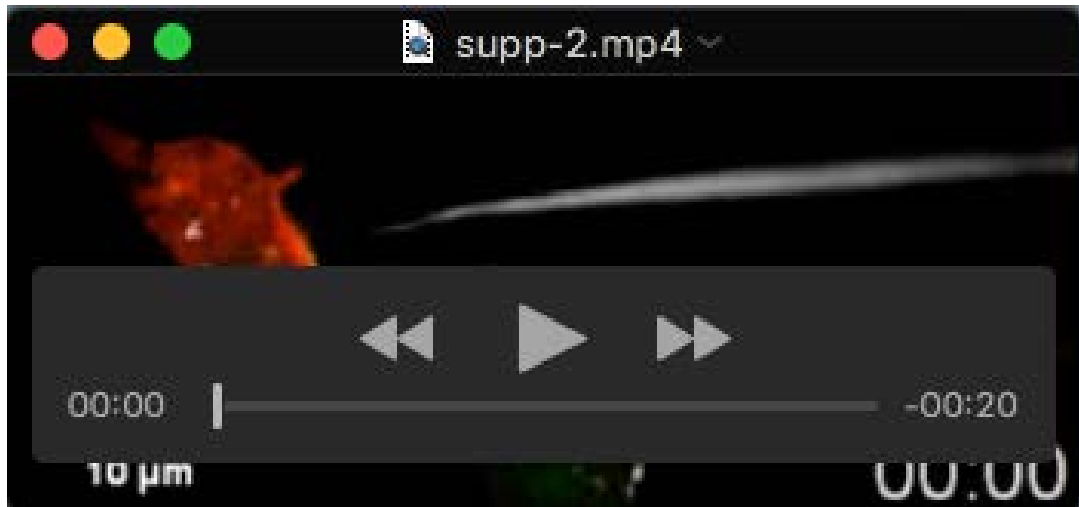
**Table S2. Strain list.**

Strain name	Genotype	Background	Source or reference
AX2		AX2	Lab stock
AX3		AX3	NBRP
<i>sgcΔ</i>	<i>sgcAΔ</i>	AX2	this study
<i>gcΔ</i>	<i>sgcAΔ, gcAΔ</i>	AX3	Veltman et al., 2006
<i>pi3k1Δ/pi3k2Δ</i>	<i>pikAΔ, pikBΔ</i>	AX2	Kamimura et al., 2016
<i>gbpAΔ</i>	<i>pdeDΔ</i>	AX3	Bosgraaf et al., 2002
<i>gbpABΔ</i>	<i>pdeDΔ, pdeEΔ</i>	AX3	Bosgraaf et al., 2002
<i>gbpCΔ</i>	<i>gbpCΔ</i>	AX3	Bosgraaf et al., 2002
<i>gbpDΔ</i>	<i>gbpDΔ</i>	AX3	Bosgraaf et al., 2002
<i>mhcAΔ</i>	<i>mhcAΔ</i>	AX3	Ruppel et al., 1994
<i>arcB</i>	<i>arcB(I191L/D197Y/K206V/A213V/F223L/P224S/E232G/I237T/H245L/S250S)</i>	AX2	Langridge and Kay, 2007
PH <sub>PKB</sub> -eGFP, sGC <sub>N</sub> -Halo7/AX2		AX2	this study
sGC-GFP/mRFP-LimEΔcoil /AX2		AX2	this study
sGC-GFP/AX2		AX2	this study
mRFP-LimEΔcoil/AX3		AX3	this study
sGCΔN-Halo7/ <i>sgcΔ</i>	<i>sgcAΔ</i>	<i>sgcΔ</i>	this study
PH <sub>PKB</sub> -eGFP, sGCΔN-Halo7 / <i>sgcΔ</i>	<i>sgcAΔ</i>	<i>sgcΔ</i>	this study
sGC-GFP/ <i>gcΔ</i>	<i>sgcAΔ, gcAΔ</i>	<i>gcΔ</i>	Sato et al., 2009

NBRP, National BioResource Project in Japan.

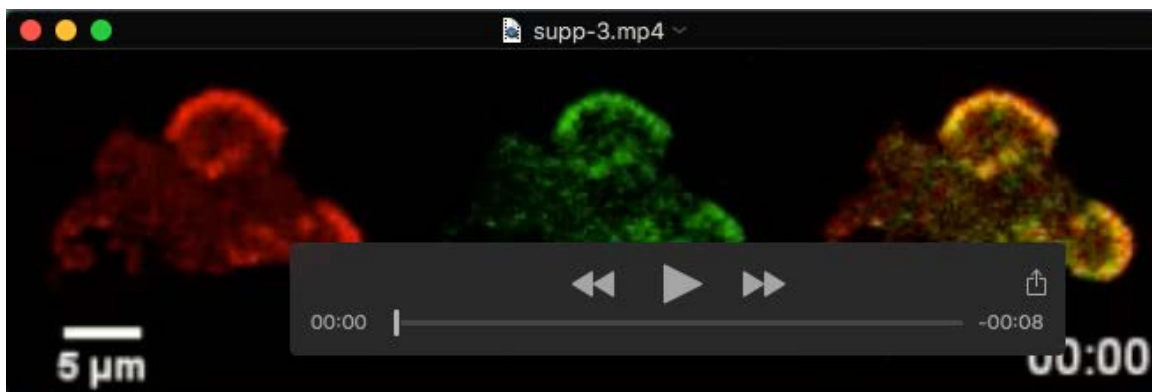


Strain name	Genotype	Background	Source or reference
sGCΔcat-GFP/ <i>gc</i> Δ	<i>sgcA</i> Δ, <i>gcA</i> Δ	<i>gc</i> Δ	Sato et al., 2009
mRFP-LimEΔcoil/ <i>gc</i> Δ	<i>sgcA</i> Δ, <i>gcA</i> Δ	<i>gc</i> Δ	this study
sGC-GFP/ <i>pi3k1</i> Δ2Δ	<i>pikA</i> Δ, <i>pikB</i> Δ	<i>pi3k1</i> Δ / <i>pi3k2</i> Δ	this study
sGC-GFP/ <i>gbpA</i> Δ	<i>pdeD</i> Δ	<i>gbpA</i> Δ	this study
mRFP-LimEΔcoil/ <i>gbpA</i> Δ	<i>pdeD</i> Δ	<i>gbpA</i> Δ	this study
mRFP-LimEΔcoil/GbpA-eGFP / <i>gbpA</i> Δ	<i>pdeD</i> Δ	<i>gbpA</i> Δ	this study
sGC-GFP/ <i>gbpAB</i> Δ	<i>pdeD</i> Δ, <i>pdeE</i> Δ	<i>gbpAB</i> Δ	this study
sGC-GFP/ <i>gbpC</i> Δ	<i>gbpC</i> Δ	<i>gbpC</i> Δ	this study
GbpC/ <i>gbpC</i> Δ	<i>gbpC</i> Δ	<i>gbpC</i> Δ	van Egmond et al., 2008
GbpCΔcGMP/ <i>gbpC</i> Δ	<i>gbpC</i> Δ	<i>gbpC</i> Δ	van Egmond et al., 2008
GbpCΔkinase/ <i>gbpC</i> Δ	<i>gbpC</i> Δ	<i>gbpC</i> Δ	van Egmond et al., 2008
mRFP-LimEΔcoil/ <i>gbpC</i> Δ	<i>gbpC</i> Δ	<i>gbpC</i> Δ	this study
sGC-GFP/ <i>gbpD</i> Δ	<i>gbpD</i> Δ	<i>gbpD</i> Δ	this study
sGC-GFP/ <i>mhcA</i> Δ	<i>mhcA</i> Δ	<i>mhcA</i> Δ	this study
sGC-GFP/ <i>arcB</i>	<i>arcB</i> (I191L/D197Y/K206 V/A213V/F223L/P224S/ E232G/I237T/H245L/S2 50S)	<i>arcB</i>	this study



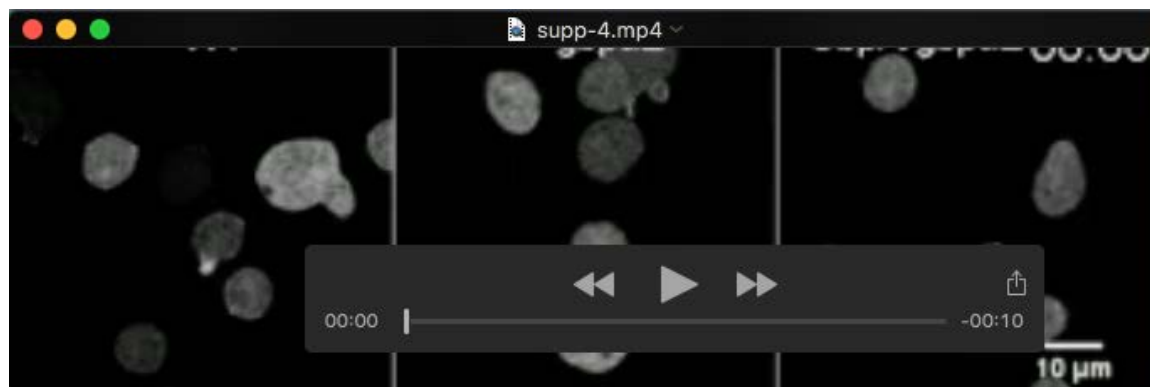
**Movie 1. Chemotactic sGC and PIP3 responses under a cAMP gradient.**

Wild-type AX2 cells expressing PH<sub>PKB</sub>-GFP (green) and sGC<sub>N</sub>-TMR (red) were stimulated with a pipette containing 40 nM cAMP. The position of the pipette (grey) was controlled by hand manipulation. The video was captured every 5 sec and is shown at 10 frame/sec. Time format is “mm:ss”.



**Movie 2. Wavelike pattern of sGC and F-actin localization.**

A wild-type AX2 cell expressing sGC-GFP and mRFP-LimEΔcoil was pretreated with 1 µM LatA for 30 min. The bottom layer of the cell was observed by confocal microscopy at 5-sec intervals. Time format is “mm:ss”.



**Movie 3. F-actin responses to 10 nM cAMP, related to Fig. 5.**

mRFP-LimE $\Delta$ coil was observed in wild-type AX3, *gpbA1*, and GbpA-eGFP-expressing *gpbA1* cells. cAMP was added at 30 sec. The video was captured every 5 sec and is shown at 12 frame/sec. Time format is “mm:ss”.



**Movie 4. F-actin response in *gcA* and *gpbCA* cells.**

mRFP-LimE $\Delta$ coil-expressing *gcA* and *gpbCA* cells were stimulated with 10 nM cAMP. The video was captured every 5 sec and is shown at 12 frame/sec. Time format is “mm:ss”.

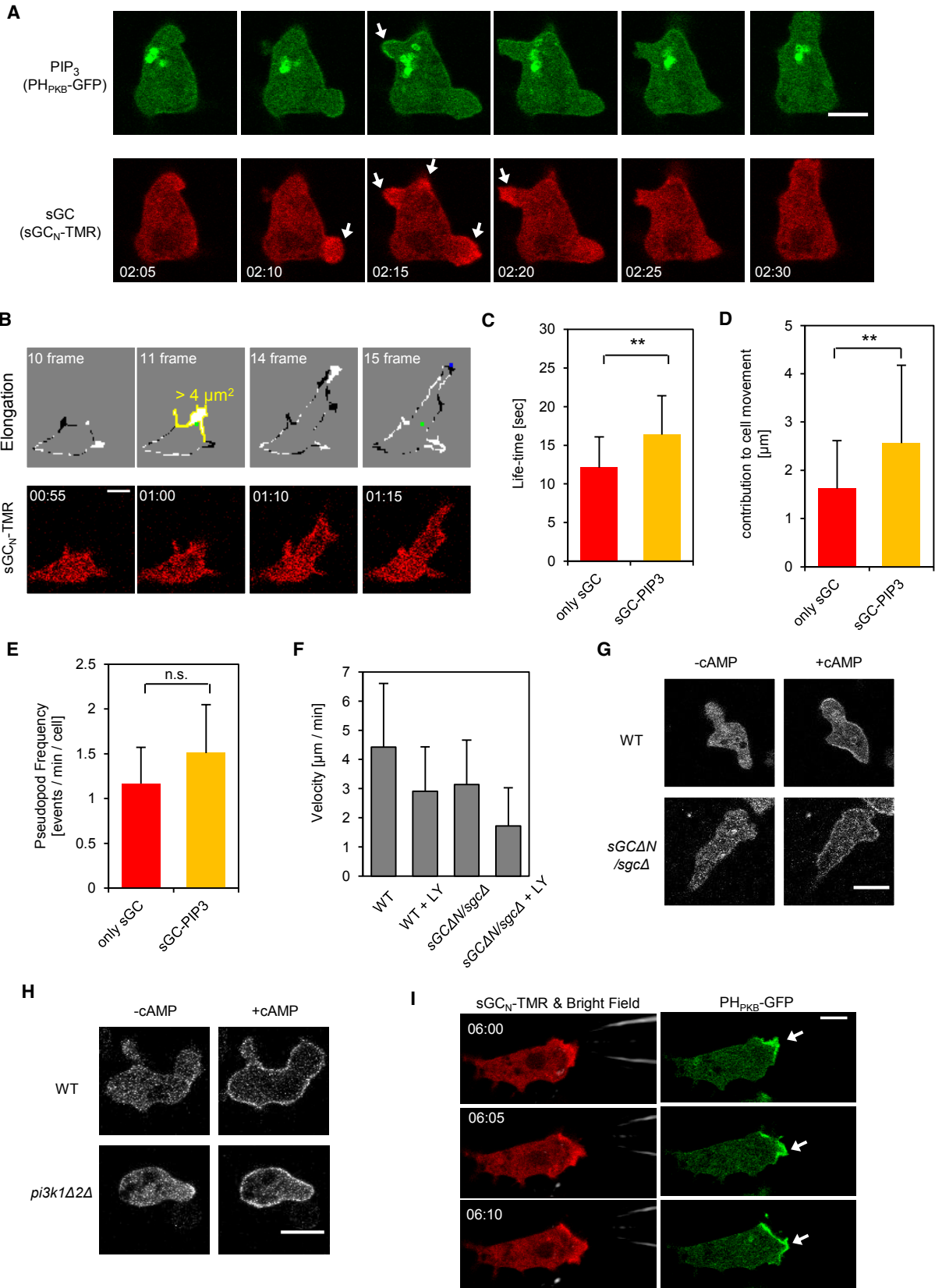


**Fig. S1. Independent function of parallel pathways**

(A) The time evolution of pseudopod dynamics shown in Figure 1A. sGC and PIP3 localizations are indicated by white arrows. (B) A representative pseudopod analysis. The fluorescence image of a cell with sGC<sub>N</sub>-TMR, shown in the bottom, was binarized and subtracted in two consecutive frames. The white and black colors in the upper panel show the positive and negative changes, respectively. An area more than 4  $\mu\text{m}^2$  (shown by the yellow ROI) was defined as a pseudopod and was pursued when it stopped expanding. The green and blue dots show the start and end points of the pseudopod, respectively. (C) The life-time of pseudopods with sGC alone or with the co-localization of sGC and PIP3 (mean + s.d. for n = 147 and 189 pseudopods, respectively). (D) Contribution to cell movement for pseudopods with sGC alone or with the co-localization of sGC and PIP3 (mean + s.d. for n = 147 and 189 pseudopods, respectively). (E) Frequencies of pseudopod formation with sGC alone or with the co-localization of sGC and PIP3. The number of pseudopods was counted if the elongation area was over 4  $\mu\text{m}^2$  (mean + s.d. for n = 13 cells). (F) Migration velocity of wild-type AX2 and *sgcA* cells expressing sGC $\Delta$ -Halo was analyzed in the presence or absence of 50  $\mu\text{M}$  LY294002 (see Methods). (G and H) PIP3 and sGC responses of the indicated cell lines at 1  $\mu\text{M}$  cAMP. PIP3 production of wild-type AX2 and sGC $\Delta$  / *sgcA* cells (G) and sGC localization of wild-type AX2 and *pi3k1A2A* cells (H) were observed by the expression of PH<sub>PKB</sub>-GFP and sGC-GFP, respectively. (I) Image galleries of a cell with sGC (red) and PIP3 (green) signals taken from supplementary Movie 1. The elongating pseudopod is shown by white arrows. Time format is “mm:ss”. Scale bars are 5 and 10  $\mu\text{m}$  in (A)-(C) and (H)-(I), respectively (\*\* P < 0.01, t-test).

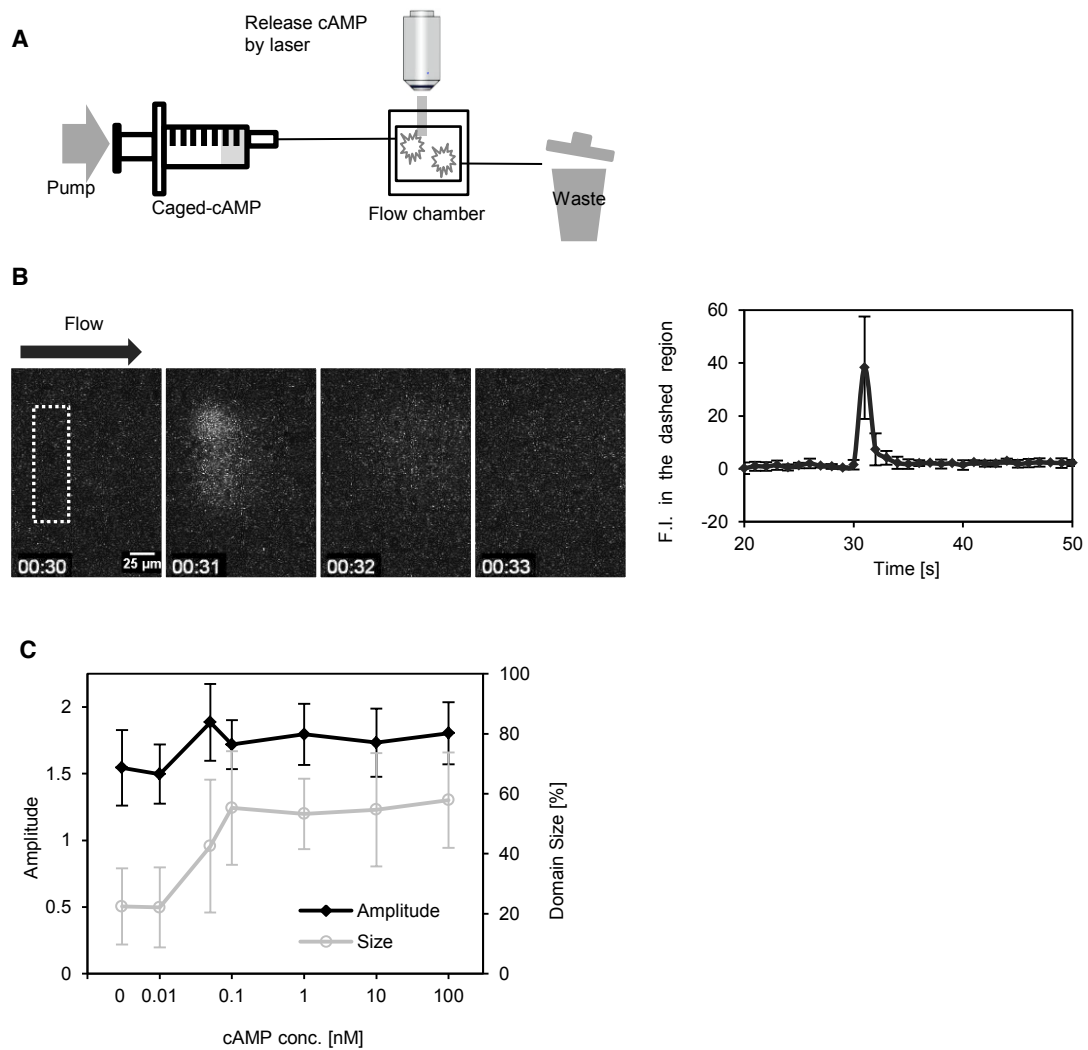


**Fig. S2. Construction of the cAMP pulse stimulation system**

(A) A schematic drawing of the pulse stimulation system. (B) Time course of the transient release of caged compound. Photolysis of 100 μM caged fluorescein in solution was carried out at the dashed region by UV flash (left). Fluorescence intensity of the region where UV was irradiated (right) (mean ± s.d. for n = 3). (C) *gcA* cells expressing sGC-GFP were stimulated with various cAMP concentrations. Response amplitude and domain size of the sGC-enriched region are shown as functions of cAMP concentrations. (mean ± s.d. for at least 8 cells).

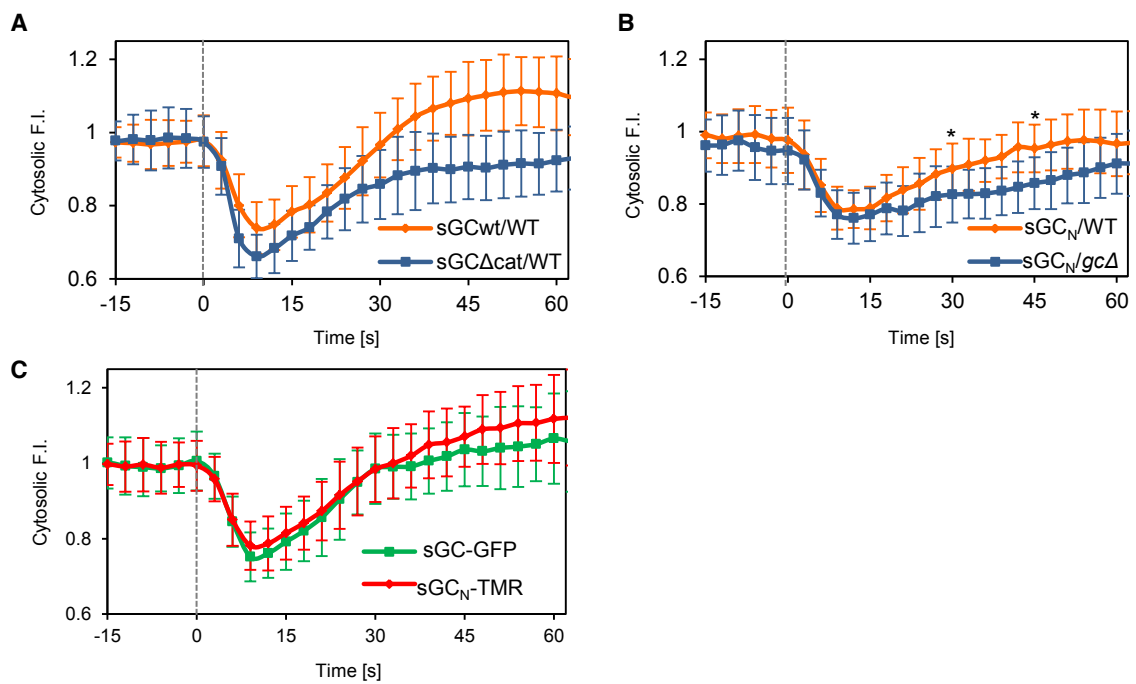


### Fig. S3. Evaluation of various sGC constructs

(A) sGC responses of the indicated cell lines upon cAMP stimulation. Wild-type AX3 cells expressing sGC<sub>WT</sub>-GFP or sGC<sub>Δcat</sub>-GFP were stimulated with 100 nM cAMP. Cytosolic intensity was normalized to the pre-stimulus level (mean  $\pm$  s.d. for at least  $n = 19$  cells). For sGC<sub>WT</sub>-GFP, the same data is shown in Figure 4C. (B) The responses of the N terminus of sGC (sGC<sub>N</sub>) in wild-type or *gcΔ* cells were observed as in (A) (mean  $\pm$  s.d. for  $n = 29$  and  $28$  cells, respectively; \*  $P < 0.01$  versus wild-type cell at 30 and 45 sec, t-test). (C) The responses of the full-length (sGC) and the N-terminal sGC (sGC<sub>N</sub>) in the same wild-type cell were observed as in (A) (mean  $\pm$  s.d. for  $n = 19$  cells).



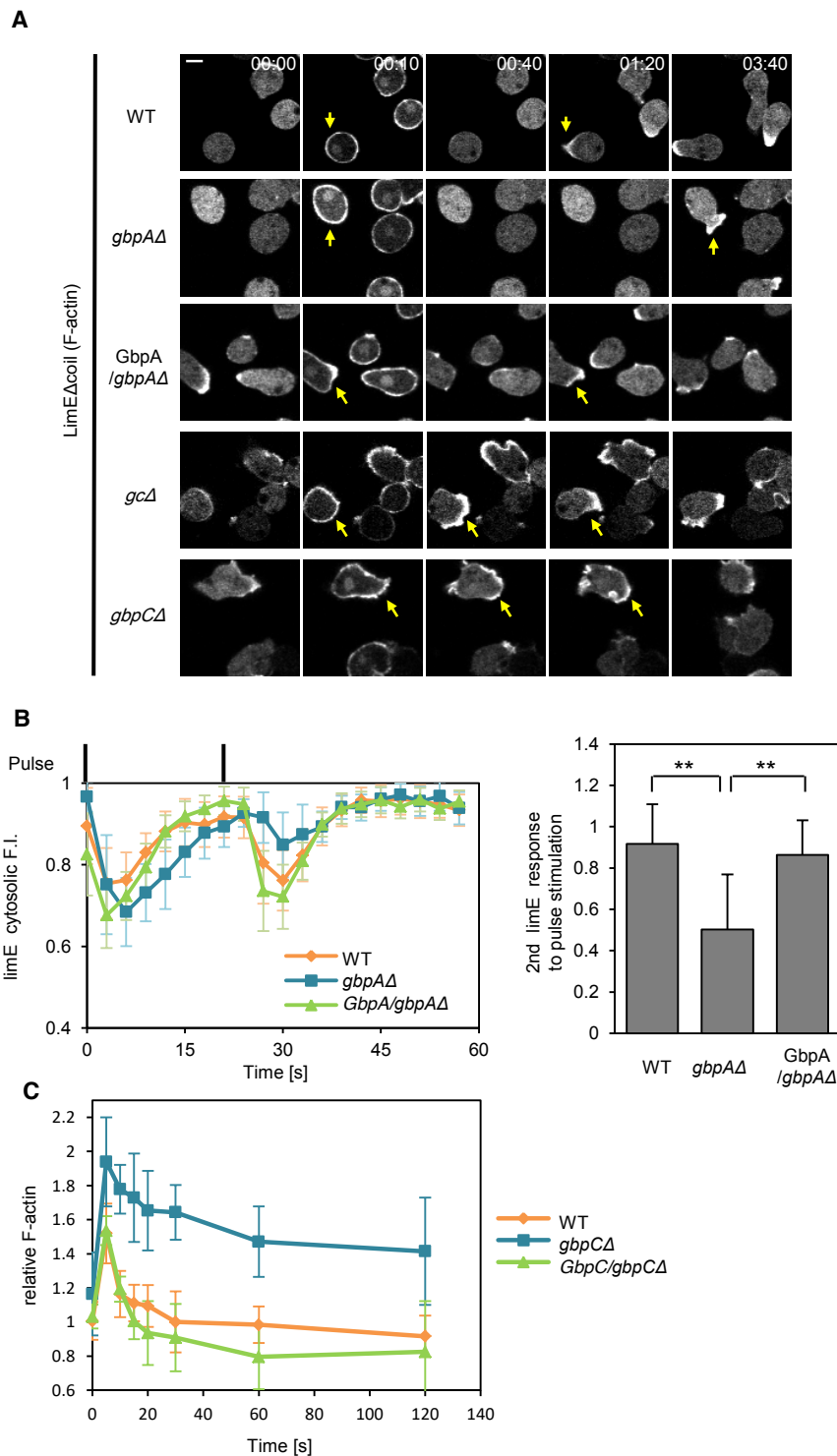


**Fig. S4. The recovery time of F-actin response depends on cGMP concentration**

(A) Wild-type AX3 and mutant cell lines expressing mRFP-LimE $\Delta$ coil were stimulated with 10 nM cAMP. Yellow arrows show the pseudopods where mRFP-LimE $\Delta$ coil localized. These pictures were clipped from Movies 3 and 4. (B) The refractoriness of F-actin depends on the amount of intracellular cGMP. Wild-type AX3, *gbpA $\Delta$*  and *gbpA $\Delta$*  rescued by GbpA cells expressing mRFP-LimE $\Delta$ coil were repetitively stimulated with 21-sec interval pulses (left) (mean  $\pm$  s.d. for  $n = 23$  cells). Cytosolic responses to 21-sec interval stimuli were normalized by the maximum fluorescence value in the time course. Black bars on the abscissa represent the pulse timing. The second responses normalized by the first responses of each cell line are shown (right) (mean + s.d.; \*\*  $P < 0.001$ , t-test). (C) Cytoskeletal F-actin amounts upon 10 nM cAMP shown in Figure 5D were normalized to the value of wild-type cells at 0 sec (mean  $\pm$  s.d. for at least 3 experiments).

**Table S1. Plasmid list.**

Plasmid name	Protein expressed	Tag	Backbone	Source or reference
sGC-GFP	SgcA	GFP	pMB74	Veltman et al., 2005
sGC $\Delta$ cat-GFP	SgcA(D1106A)	GFP	pMB74	Veltman et al., 2006
sGCN-Halo7	SgcA(1-1019)	Halo7	pHK12	this study
sGC $\Delta$ N-Halo7	SgcA(877-2843)	Halo7	pHK12	this study
PH <sub>PKB</sub> -eGFP	PkbA(1-113)	eGFP	pBIG	Meili et al., 1999
mRFP-LimE $\Delta$ coil	LimE(1-145)	mRFP	pHK12	this study
GbpA-eGFP	GbpA	eGFP	pDM358	this study

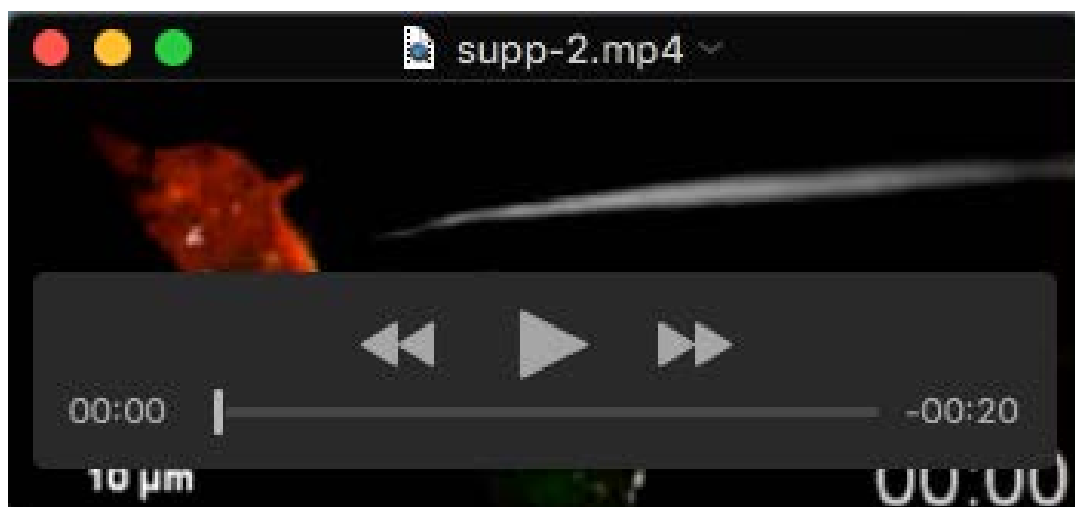
Numbers in parentheses refer to a mutation or regions of amino acid residues.

**Table S2. Strain list.**

Strain name	Genotype	Background	Source or reference
AX2		AX2	Lab stock
AX3		AX3	NBRP
<i>sgcΔ</i>	<i>sgcAΔ</i>	AX2	this study
<i>gcΔ</i>	<i>sgcAΔ, gcAΔ</i>	AX3	Veltman et al., 2006
<i>pi3k1Δ/pi3k2Δ</i>	<i>pikAΔ, pikBΔ</i>	AX2	Kamimura et al., 2016
<i>gbpAΔ</i>	<i>pdeDΔ</i>	AX3	Bosgraaf et al., 2002
<i>gbpABΔ</i>	<i>pdeDΔ, pdeEΔ</i>	AX3	Bosgraaf et al., 2002
<i>gbpCΔ</i>	<i>gbpCΔ</i>	AX3	Bosgraaf et al., 2002
<i>gbpDΔ</i>	<i>gbpDΔ</i>	AX3	Bosgraaf et al., 2002
<i>mhcAΔ</i>	<i>mhcAΔ</i>	AX3	Ruppel et al., 1994
<i>arcB</i>	<i>arcB(I191L/D197Y/K206V/A213V/F223L/P224S/E232G/I237T/H245L/S250S)</i>	AX2	Langridge and Kay, 2007
PH <sub>PKB</sub> -eGFP, sGC <sub>N</sub> -Halo7/AX2		AX2	this study
sGC-GFP/mRFP-LimEΔcoil /AX2		AX2	this study
sGC-GFP/AX2		AX2	this study
mRFP-LimEΔcoil/AX3		AX3	this study
sGCΔN-Halo7/ <i>sgcΔ</i>	<i>sgcAΔ</i>	<i>sgcΔ</i>	this study
PH <sub>PKB</sub> -eGFP, sGCΔN-Halo7 / <i>sgcΔ</i>	<i>sgcAΔ</i>	<i>sgcΔ</i>	this study
sGC-GFP/ <i>gcΔ</i>	<i>sgcAΔ, gcAΔ</i>	<i>gcΔ</i>	Sato et al., 2009

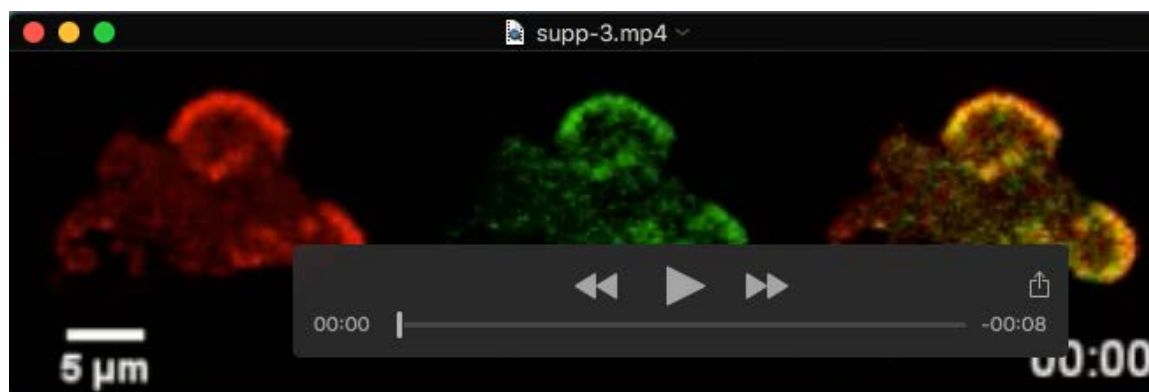
NBRP, National BioResource Project in Japan.

Strain name	Genotype	Background	Source or reference
sGCΔcat-GFP/ <i>gc</i> Δ	<i>sgcA</i> Δ, <i>gcA</i> Δ	<i>gc</i> Δ	Sato et al., 2009
mRFP-LimEΔcoil/ <i>gc</i> Δ	<i>sgcA</i> Δ, <i>gcA</i> Δ	<i>gc</i> Δ	this study
sGC-GFP/ <i>pi3k1</i> Δ <i>2</i> Δ	<i>pikA</i> Δ, <i>pikB</i> Δ	<i>pi3k1</i> Δ / <i>pi3k2</i> Δ	this study
sGC-GFP/ <i>gbpA</i> Δ	<i>pdeD</i> Δ	<i>gbpA</i> Δ	this study
mRFP-LimEΔcoil/ <i>gbpA</i> Δ	<i>pdeD</i> Δ	<i>gbpA</i> Δ	this study
mRFP-LimEΔcoil/GbpA-eGFP / <i>gbpA</i> Δ	<i>pdeD</i> Δ	<i>gbpA</i> Δ	this study
sGC-GFP/ <i>gbpAB</i> Δ	<i>pdeD</i> Δ, <i>pdeE</i> Δ	<i>gbpAB</i> Δ	this study
sGC-GFP/ <i>gbpC</i> Δ	<i>gbpC</i> Δ	<i>gbpC</i> Δ	this study
GbpC/ <i>gbpC</i> Δ	<i>gbpC</i> Δ	<i>gbpC</i> Δ	van Egmond et al., 2008
GbpCΔcGMP/ <i>gbpC</i> Δ	<i>gbpC</i> Δ	<i>gbpC</i> Δ	van Egmond et al., 2008
GbpCΔkinase/ <i>gbpC</i> Δ	<i>gbpC</i> Δ	<i>gbpC</i> Δ	van Egmond et al., 2008
mRFP-LimEΔcoil/ <i>gbpC</i> Δ	<i>gbpC</i> Δ	<i>gbpC</i> Δ	this study
sGC-GFP/ <i>gbpD</i> Δ	<i>gbpD</i> Δ	<i>gbpD</i> Δ	this study
sGC-GFP/ <i>mhcA</i> Δ	<i>mhcA</i> Δ	<i>mhcA</i> Δ	this study
sGC-GFP/ <i>arcB</i>	<i>arcB</i> (I191L/D197Y/K206 V/A213V/F223L/P224S/ E232G/I237T/H245L/S2 50S)	<i>arcB</i>	this study



**Movie 1. Chemotactic sGC and PIP3 responses under a cAMP gradient.**

Wild-type AX2 cells expressing PH<sub>PKB</sub>-GFP (green) and sGC<sub>N</sub>-TMR (red) were stimulated with a pipette containing 40 nM cAMP. The position of the pipette (grey) was controlled by hand manipulation. The video was captured every 5 sec and is shown at 10 frame/sec. Time format is “mm:ss”.



**Movie 2. Wavelike pattern of sGC and F-actin localization.**

A wild-type AX2 cell expressing sGC-GFP and mRFP-LimEΔcoil was pretreated with 1 μM LatA for 30 min. The bottom layer of the cell was observed by confocal microscopy at 5-sec intervals. Time format is “mm:ss”.



**Movie 3. F-actin responses to 10 nM cAMP, related to Fig. 5.**

mRFP-LimE $\Delta$ coil was observed in wild-type AX3, *gbpA1*, and GbpA-eGFP-expressing *gbpA1* cells. cAMP was added at 30 sec. The video was captured every 5 sec and is shown at 12 frame/sec. Time format is “mm:ss”.



**Movie 4. F-actin response in *gcA* and *gbpCA* cells.**

mRFP-LimE $\Delta$ coil-expressing *gcA* and *gbpCA* cells were stimulated with 10 nM cAMP. The video was captured every 5 sec and is shown at 12 frame/sec. Time format is “mm:ss”.